APPLIED PHYSICS REVIEWS—FOCUSED REVIEW

Size effects and charge transport in metals: Quantum theory of the resistivity of nanometric metallic structures arising from electron scattering by grain boundaries and by rough surfaces

Raul C. Munoz[1] and Claudio Arenas[2]
[1]*Departamento de Fisica, Facultad de Ciencias Fisicas y Matematicas, Universidad de Chile, Blanco Encalada 2008, Casilla 487-3, Santiago 8370449, Chile*
[2]*Synopsys, Inc., Avenida Vitacura 5250, Oficina 708, Vitacura, Santiago, Chile*

(Received 5 August 2016; accepted 7 November 2016; published online 2 February 2017)

We discuss recent progress regarding size effects and their incidence upon the coefficients describing charge transport (resistivity, magnetoresistance, and Hall effect) induced by electron scattering from disordered grain boundaries and from rough surfaces on metallic nanostructures; we review recent measurements of the magneto transport coefficients that elucidate the electron scattering mechanisms at work. We review as well theoretical developments regarding quantum transport theories that allow calculating the increase in resistivity induced by electron-rough surface scattering (in the absence of grain boundaries) from first principles—from the parameters that describe the surface roughness that can be measured with a Scanning Tunnelling Microscope (STM). We evaluate the predicting power of the quantum version of the Fuchs-Sondheimer theory and of the model proposed by Calecki, abandoning the method of parameter fitting used for decades, but comparing instead theoretical predictions with resistivity measured in thin films where surface roughness has also been measured with a STM, and where electron-grain boundary scattering can be neglected. We also review the theory of Mayadas and Shatzkes (MS) [Phys. Rev. B **1**, 1382 (1970)] used for decades, and discuss its severe conceptual difficulties that arise out of the fact that: (i) MS employed plane waves to describe the electronic states within the metal sample having periodic grain boundaries, rather than the Bloch states known since the thirties to be the solutions of the Schrödinger equation describing electrons propagating through a Krönig-Penney [Proc. R. Soc. London Ser. A **130**, 499 (1931)] periodic potential; (ii) MS ignored the fact that the wave functions describing electrons propagating through a 1-D disordered potential are expected to decay exponentially with increasing distance, a fact known since the work of Anderson [Phys. Rev. **109**, 1492 (1958)] in 1958 for which he was awarded the Nobel Prize in 1977; (iii) The current in the sample should be proportional to T_N, the probability that an electron traverses N consecutive (disordered) grains found along a mean free path; MS assumed that $T_N = 1$. We review unpublished details of a quantum transport theory based upon a model of diffusive transport and Kubo's linear response formalism recently published [Arenas *et al.*, Appl. Surf. Sci. **329**, 184 (2015)], which permits estimating the increase in resistivity of a metallic specimen (over the bulk resistivity) under the combined effects of electron scattering by phonons, impurities, disordered grain boundaries, and rough surfaces limiting the sample. We evaluate the predicting power of both the MS theory and of the new quantum model on samples where the temperature dependence of the resistivity has been measured between 4 K and 300 K, and where surface roughness and grain size distribution has been measured on each sample via independent experiments. We find that the quantum theory does exhibit a predicting power, whereas the predicting power of the MS model as well as the significance and reliability of its fitting parameters seems questionable. We explore the power of the new theory by comparing, for the first time, the resistivity predicted and measured on nanometric Cu wires of (approximately) rectangular cross section employed in building integrated circuits, based upon a quantum description of electron motion. *Published by AIP Publishing.* [http://dx.doi.org/10.1063/1.4974032]

TABLE OF CONTENTS

I. INTRODUCTION 2
II. THEORY 4
A. The resistivity of a crystalline metal 4
B. Classical theories of electron-rough surface scattering in thin metallic films 5
1. Theory of Fuchs and Sondheimer 5
2. Theory of Calecki 6

3. Including the effect of electron-phonon plus electron-impurity scattering in the formalism of Calecki 7
C. Quantum theories of electron-surface scattering 7
1. Theory of Tesanovic, Jaric, and Maekawa (TJM) 7
2. Theory of Trivedi and Aschroft (TA) ... 7
3. Theory of Sheng, Xing, and Wang (SXW) 8
4. Quantum version of the Fuchs-Sondheimer model: Modified theory of Sheng, Xing, and Wang (mSXW) 8
5. Determination of the bulk resistivity $\boldsymbol{\rho}_0$ and bulk mean free path ℓ_0, using as input the surface roughness data (δ, ξ) .. 9
6. Quantum theory of resistivity arising from electrons colliding with a rough fractal surface 9
D. Classical theory of electron-grain boundary scattering 10
1. Theory of Mayadas and Shatzkes (MS) .. 10
2. Conceptual difficulties and inconsistencies of the theory of Mayadas and Shatzkes 12
E. Quantum theory of electron-grain boundary scattering 13
1. Solutions of Schrödinger equation for the Krönig-Penney potential 13
2. Conductivity of a crystalline sample containing uniform, equally spaced grain boundaries 14
3. Conductivity of a thin film bounded by two flat surfaces 14
4. Conductivity of a wire of rectangular cross section bounded by flat surfaces ... 14
5. Effect of disorder 14
6. Estimation of the transmission coefficient T_N 15
7. Contribution to the resistivity of a thin film arising from energy dissipation involved in electron-rough surface scattering 16
III. SIZE EFFECTS IN THE PRESENCE OF A MAGNETIC FIELD 17
A. Hall voltage 17
B. Hall tangent and Hall mobility 18
C. Magnetoresistance 19
IV. RESISTIVITY DATA AND PREDICTIONS OF THEORIES OF ELECTRON-SURFACE SCATTERING (IN THE ABSENCE OF GRAINS) 20
A. Predictive power of the Fuchs-Sondheimer theory 20
B. Predictive power of Calecki's theory 20
C. Predictive power of the quantum transport theories 21
1. Determination of the height-height autocorrelation function from precision measurements of the surface topography employing a STM 21
2. Interference between electron scattering in the bulk and electron-surface scattering, and violations of Mathiessen's rule 21
3. The bulk resistivity 23
V. RESISTIVITY DATA AND PREDICTIONS OF THEORIES OF ELECTRON-GRAIN BOUNDARY SCATTERING 24
A. Predictive power of the theory of Mayadas and Shatzkes, and of the quantum theory of electron-grain boundary scattering 26
VI. ESTIMATION OF THE RESISTIVITY OF NANOMETRIC CU WIRES OF RECTANGULAR CROSS SECTION 28
VII. DISCUSSION 29
A. Electron-surface scattering or electron-grain boundary scattering? 29
B. Is the resistivity arising from electron-phonon scattering also affected by "size effects"? 30
C. Modeling of nanoscale devices: Ballistic transport or diffusive transport? 30
D. Shortcomings of the quantum theory of electron-grain boundary scattering 32
1. The texture of grain boundaries 32
2. The effect of molecules present on a metallic rough surface 32

I. INTRODUCTION

Ever since the construction of the first integrated circuits (IC's) in the late fifties, an effort to increase the speed of the ICs by decreasing the linear dimensions of its components has been made, in what today is known as Ultra Large Scale Integration (ULSI). This gave rise to a relation proposed in 1965 by Gordon Moore—cofounder of INTEL—according to which, the number of transistors per unit area on a Si wafer approximately doubled every 2 years.

One of the assumptions underlying this relation is that the resistivity of the metallic lines that connect the transistors in an IC remains the same as the linear dimensions shrink. For over 4 decades, the model used to estimate the resistivity of the interconnects was based upon the classical theory of resistivity of thin metallic films published by Mayadas and Shatzkes (MS).[1] Nevertheless, INTEL announced in March 2016 that "Moore's law" is coming to a halt, because the resistivity of Cu interconnects—the metal used by the electronic industry over the last two decades to connect the transistors in an IC—turns out to increase with shrinking dimensions (and is dominated by quantum effects), when the width and/or the height of the metallic connector becomes smaller than $\ell_0(300) = \ell_{Cu}(300) = 38\,\text{nm}$, the intrinsic electronic mean free path in crystalline Cu at 300 K arising from electron-phonon scattering. Understanding why the resistivity increases with shrinking dimensions has remained a stumbling

block, for the classical MS theory (based upon solutions of the Boltzmann Transport Equation, BTE) does not describe properly the underlying quantum effects.

The development of the electronic industry worldwide poses a pressing need to reach a satisfactory understanding of size effects. Progress in the manufacturing of integrated circuits has led to ULSI, to a decrease of the linear dimensions of connecting lines, such that the width of interconnects is now comparable to or smaller than $\ell_{Cu}(300)$. There are recent reports that point to the fact that: (i) The wire width expected for the next decade is rapidly approaching about 10 nm, a dimension which is about one order of magnitude larger than the electronic Fermi wave length in Cu, and is about 25% of $\ell_{Cu}(300)$. (ii) At these short scales, Moore's empirical law is expected to come to a halt,[2–5] because quantum effects are expected to dominate charge transport. At scales smaller than $\ell_{Cu}(300)$, a quantum description of electron motion seems essential.

The scientific community interested in size effects in nanometric interconnects has shifted sides, regarding the estimation of the resistivity of metallic interconnects. After using the classical theory of Mayadas and Shatzkes for decades without questioning the underlying physical description of electron transport, there is a recent report where charge transport across Cu wires (having a diameter of the order of 3 nm or smaller) is *computed using the formalism of Büttiker and Landauer,* that is, assuming that electron motion within the wire is well described by a model of *ballistic transport*.[6] This is a quantum model appropriate for describing electron motion in semiconducting structures (grown using molecular beam epitaxy) cooled to 4 K, where the sample has a very small amount of impurities/structural defects and the phonons are frozen out. It seems questionable whether predictions based upon *ballistic transport* could ever describe appropriately charge transport at room temperature in nanometric Cu wires having a length larger than about $2.5\ell_0(300) \approx 100$ nm; in wires of such dimensions, electron scattering from structural defects (such as disordered grain boundaries (GB), impurities, and phonons) are expected to play a significant role. We return to this point at the end of this work.

We published *a quantum theory of the resistivity of nanometric metallic interconnects* that provides a coherent and self-consistent explanation of why the resistivity increases with shrinking dimensions.[7] The interesting result is that, contrary to the classical MS theory—that has a highly questionable predicting power, as will be discussed below—the quantum theory does exhibit a predicting power. Theoretical predictions were compared to resistivity data in gold films. In samples where the grain diameter is of the order of 11 nm, the resistivity measured at 300 K turns out to be about an order of magnitude larger than the resistivity of crystalline gold at the same temperature. According to the new theory, such an increase in resistivity is dominated by weak Anderson localization induced by electron scattering from disordered grain boundaries, and the Anderson localization length controlling the resistivity on these small grained samples turns out to be about 110 nm. Beyond the fact that this quantum theory provides a coherent theoretical description of electron motion valid at these short length scales, there is another significant advantage of the new quantum theory that is worth mentioning: It allows a straightforward calculation of the resistivity of wires of approximately rectangular cross section from first principles, using the Green's function built from the known solutions of the Schrödinger equation describing an electron gas confined in two dimensions. This is in contrast to the MS theory, where—apart from the severe conceptual difficulties of the theory, that results in its questionable predicting power—the solution of BTE for wires of rectangular cross section remains unknown.

For these reasons, and because: (i) our quantum transport theory is based upon *diffusive transport* (rather than ballistic transport), (ii) because the theory allows a straightforward rough estimation of the resistivity of nanometric wires of rectangular cross section *including the effect of disorder*, *of grain boundaries, of electron-phonon scattering*, *and of electron-impurity/point defect scattering,* we decided to undertake the task of briefly reviewing both theoretical as well as experimental work regarding charge transport in nanometric metallic structures that has taken place over the last two decades, *leading to a quantum description of charge transport that enjoys a predicting power,* as will be discussed below. This paper contains unpublished information leading to the quantum theory of Ref. 7.

However, before addressing the quantum description of the resistivity arising from these two electron scattering mechanisms (electron-surface and electron grain boundary scattering), a critical review of the main theories that have been used for decades to describe size effects seems in order: the theory of Fuchs-Sondheimer (FS) and the theory of Mayadas and Shatzkes (MS). In this context, it seems appropriate to mention that a quantum version of FS theory is available.

However, the process of comparing theoretical predictions with resistivity data has been based for decades upon parameter fitting employing some sweeping assumptions; the validity of these assumptions and the values of the fitting parameters today seem questionable—thanks to technical improvements and to new tools such as the Scanning Tunneling Microscope (STM). Consequently, we consider that such a review ought to address an evaluation of the predicting power of quantum theories of resistivity *abandoning the process based upon parameter fitting regarding the effect of electron scattering by rough surfaces (RS) and by grain boundaries,* but comparing instead theoretical predictions with resistivity data *in samples where the surface roughness is no longer considered an adjustable parameter, but where the surface roughness and grain size distribution have been measured through independent experiments*. Such a critical evaluation of existing charge transport theories based upon surface roughness data and grain size distribution data measured through independent experiments (abandoning the method of parameter fitting) seems timely, for it does not seem to have been published.

It seems appropriate to point out that there is additional useful information obtained by measuring transport coefficients in the presence of a magnetic field. This information has helped to elucidate the nature of the microscopic electron

scattering mechanisms at work that are responsible for the observed resistivity; such information is not always available when measuring simply the resistivity of the specimen in the absence of a magnetic field. Therefore, a critical review ought to include as well other manifestations of size effects (for example, *magnetoresistance and Hall effect measured together with the resistivity in the absence of a magnetic field*); such a discussion does not seem to have been published either.

For the reasons outlined above, the goal of this work is to review some evidence that has been published over the last two decades, from which a conceptually coherent and a satisfactory understanding of size effects using a quantum description of charge transport seems to be slowly emerging. The discussion focuses on evidence regarding charge transport in nonmagnetic metals of interest for the electronic industry, such as Al, Cu, and Au. We will focus on research that contributes to elucidate how charge transport takes place, and what are the relevant electron scattering mechanism controlling the resistivity over the short scales of distance that characterize the dimensions of the interconnects used in IC's today. We cover briefly some recent developments taking place, both experimental and theoretical, which allow identifying the electron scattering mechanisms at work. Regarding the theoretical discussion, the emphasis is focused on the description of the fundamental concepts and on some basic sweeping assumptions underlying existing theories of size effects starting from ground zero, rather than on mathematical details; the reader who is interested in the latter is referred to the original literature. For the sake of clarity, in the presentation of different topics, we have decided to include recent references that support and underline the different arguments presented in the text; a comprehensive coverage of the several hundred papers published regarding charge transport in mesoscopic metallic systems over the last two decades is beyond the scope of this focused review.

We start by pointing out that the first published evidence that charge transport in metallic samples depends not only on the metal making up the sample, but also on its size (hence the name "size effects"), appears to have been published by Isabelle Stone as a result of her Ph.D. thesis research.[8] It turns out that size effects also manifest themselves in the coefficients that describe charge transport measured in the presence of a magnetic field, such as the Hall effect and the magnetoresistance; the first experimental evidence that the size of the metal specimen *also* affects the coefficients describing magneto transport appears to have been published in the mid of the twentieth century.[9]

The paper is organized as follows. Section II is devoted to theory. This section includes, of course, a short discussion of the classical theory of Fuchs and Sondheimer as well as its quantum version, the modified theory of Sheng, Xing, and Wang (mSXW). We include as well a brief discussion of the quantum theory of resistivity (QTR) originating on electron scattering from a rough fractal surface. It includes, also, a brief discussion of the only classical theory of size effects (in the absence of grain boundaries) that is based upon the Boltzmann Transport Equation, but yet *carries no adjustable parameters*: the theory of Calecki. We present, of course, the theory of Mayadas and Shatzkes (MS) and discuss its conceptual difficulties and inconsistencies. We finish the section devoted to theory by presenting a summary of the quantum version of MS theory, the quantum theory of electron-grain boundary scattering, including several unpublished details.

Section III is devoted to experimental manifestations of size effects in the presence of a magnetic field, including the Hall voltage, the Hall tangent, the Hall mobility, and the magnetoresistance. Section IV contains a comparison between resistivity data and theoretical predictions regarding theories of electron-surface scattering (in the absence of grain boundaries), in samples where the surface roughness has been measured through independent experiments. In Section IV, we discuss the predictive power of the Fuchs-Sondheimer theory, of Calecki's theory, and of different quantum theories of electron-surface scattering. Section V is dedicated to discussing the predicting power of the classical theory of Mayadas and Shatzkes and of the quantum theory. In Section VI, we explore the power of the new quantum theory; we present an estimation of the resistivity of nanometric Cu wires of rectangular cross section used in building IC's.

We finish with Section VII, where we present a discussion regarding some of the open problems in the field, and we discuss as well the range of applicability of this new theory and how it fits within the wider picture of emerging theories aimed at modeling nanoscale devices.

II. THEORY

It seems appropriate to begin the theoretical discussion by mentioning briefly the theory of Bloch-Grüneisen, which provides an adequate description of the resistivity of a crystalline nonmagnetic metal. The theory is based upon a solution of the Boltzmann Transport Equation (BTE) employing the relaxation time (τ) approximation.

A. The resistivity of a crystalline metal

The resistivity data of crystalline metals can be well described by

$$\rho_0(T) = \rho_R + A\left(1 + \frac{BT}{\theta - CT}\right)\varphi\left(\frac{\theta - CT}{T}\right), \quad \text{with}$$
$$\varphi(x) = 4x^{-5}\int_0^x \frac{z^5 \exp(z)}{(\exp(z) - 1)^2} dz, \tag{1}$$

where A, B, C, and ρ_R are constants, $x = \theta/T$, θ is the Debye temperature characterizing the vibrational spectrum of the crystalline lattice, and T is the absolute temperature. Replacement of θ in the Bloch-Grüneisen formula by θ—CT provides for representation of changes in the effective Debye temperature due to anharmonicity of the atomic vibrations and the thermal expansion of the material.[10] The first term on the right hand side (RHS) of Equation (1) represents the residual (temperature independent) resistivity arising from electron scattering by impurities/point defects, and the second term in brackets represents the resistivity arising from electron-acoustic phonon scattering. The constant A is

proportional to the electron-phonon coupling constant that characterizes the metallic sample.

B. Classical theories of electron-rough surface scattering in thin metallic films

Classical theories are theories where electron motion is described using a BTE, that have been published to describe the increase in resistivity arising from electron-rough surface scattering, in metallic samples where grain boundaries are absent. Because of limitations of space, we restrict the discussion to the Fuchs-Sondheimer (FS) theory and to the theory published by Calecki.

1. Theory of Fuchs and Sondheimer

Sondheimer[11] published a description of size effects on thin metallic films based upon a solution of BTE that followed an idea first proposed by Fuchs,[12] which became the Fuchs-Sondheimer (FS) theory. Fuchs and Sondheimer assumed that the metallic *film was bounded by two surfaces having the same roughness*; the extension of the FS theory to a film of thickness t limited by two surfaces (oriented normal to z) having different roughness was published by Lucas.[13] We present the argument of FS, applied to a film limited by two different surfaces, for this is the situation commonly found in experimental work.

Lucas arrived at the following result:

$$\left(\frac{\rho_0}{\rho}\right) = 1 - \frac{3\ell_0}{4t}\int_0^{2\pi}\int_0^{\pi/2} \frac{\cos^2(\phi)\cos(\theta)\sin^3(\theta)[1-E(\zeta)]\left[2-p_0-p_t+(p_0+p_t-2p_0p_t)E(\zeta)\right]}{1-p_0p_tE(\varsigma)^2}\,d\theta d\phi, \tag{2}$$

$$\text{with } \ell_0 = v_F\tau, \zeta = \sin(\theta)\cos(\phi), E(\zeta) = \exp\left(-\frac{t}{\ell_0\cos(\theta)}\right). \tag{3}$$

Within this model, v_F is the Fermi velocity, τ is the electronic relaxation time describing electron scattering in the bulk, $\ell_0(T)$ and $\rho_0(T)$ are the mean free path and resistivity of the bulk at temperature T. *The specularities $p_{0,t}$ are phenomenological adjustable parameters*; they represent the fraction of electrons that undergo a specular reflection upon colliding with the rough surfaces located at $z=0$ and $z=t$, respectively. Many researchers have analysed their thin film (TF) resistivity data *ignoring that the film may have two surfaces characterized by different specularities p_0 and p_t*. Under the sweeping assumption $p_0=p_t=p$, Equation (2) reduces to

$$\left(\frac{\rho_0}{\rho}\right) = \frac{\sigma}{\sigma_0} = 1 - \frac{3\ell_0}{4t}(1-p) \times \int_0^{\pi} \frac{\cos(\theta)\sin^3(\theta)\left[1-\exp\left(-t/(\cos\theta\ell_0)\right)\right]}{1-p\exp\left(-t/(\cos\theta\ell_0)\right)}d\theta. \tag{4}$$

When $p=1$, $\rho=\rho_0$. Hence, the resistivity ρ_0 of the bulk is the resistivity of a fictitious metallic film having the same concentration of impurities/point defects as the sample, but limited by two flat surfaces such that electrons colliding with them are reflected secularly; *ρ_0 is the resistivity that would be observed in the thin film if electron-surface scattering was switched off.*

Current interest in nanometric metallic connectors dictate the necessity of critically reviewing the predictions of the Fuchs-Sondheimer theory, since it is certainly the most influential theory of size effects and has guided research on the subject for several decades. In the case of ultra pure thin films the FS theory leads to $\sigma \sim \sigma_0\ (t/\ell_0)\ \ln(\ell_0/t)$, which implies that $\sigma \sim c\ t\ \ln(\ell_0/t)$, where c is a quantity that is independent of both t and ℓ_0. This means that the conductivity of metallic films where $t \ll \ell_0$ should grow as $t\ \ln(\ell_0/t)$ with increasing ℓ_0; under such conditions charge transport is dominated by electron-surface scattering. This prediction implies that σ increases (and hence the energy dissipated by electron surface scattering decreases) with increasing ℓ_0.

In the limit $\ell_0 \to \infty$ the conductivity becomes infinity, and *electron-rough surface scattering no longer dissipates energy*. Such prediction is wrong, for: (i) it contradicts the starting assumption of the theory, where electron-surface scattering is expected to contribute to the resistivity (and to energy dissipation) in the film; (ii) it contradicts the resistivity of a family of ultra pure very thin epitaxial $CoSi_2$ films measured at 4 K. The error arises from employing a classical rather than a quantum description of electron motion; it stems from the fact that electrons in a thin metallic film occupy electronic states where the electron momentum perpendicular to the surface of the film is quantized as a consequence of electron confinement between two parallel planes. The quantum nature of such electronic states has a profound influence on the description of charge transport in thin films, it leads to: (a) Interference between electron scattering taking place in the bulk and electron-surface scattering that result in violations of Mathiessen's rule (as discussed below, Section IV C 2). (b) The quantum version of FS theory involves a sum over electron states (where the electron momentum perpendicular to the surface of the film is quantized) that leads to a film conductivity σ that ia *always smaller than* the bulk conductivity σ_0, no matter how large ℓ_0 is, so energy dissipation arising from electron-rough surface scattering is well accounted for, as discussed in Section II C 4 below.

Evidence has been published suggesting that such quantum electron states dominate the conductivity of very thin

$CoSi_2$ films, for the conductivity (plotted as a function of film thickness) *decreases dramatically* with decreasing thickness for films whose thickness decreases below 10 nm. Such a dramatic decrease of conductivity seems at variance with the rather smooth variation expected from the classical FS theory. It has been reported that:

> "…It is clear that the variation of ρ versus t (thickness) cannot be represented by the Fuchs-Sondheimer theory whatever the fitting parameter p. ρ is almost constant down to 20 nm and increases dramatically as the film thickness decreases below 10 nm" (Reference 14, p. 170).

During several decades, researchers applied this over simplified model $p_0 = p_t = p$ to analyse thin film resistivity data, measured on families of *films of different thickness made out of the same material, prepared under similar experimental conditions*. However, the resistivity ρ of the film predicted by Equation (4) depends on $\ell_0(T)$ and on $\rho_0(T) = 1/\sigma_0(T)$, respectively, as well as on the reflectivity p. To carry out the data analysis, two quite strong and sweeping assumptions had to be made (beyond *the assumption that the two surfaces limiting the thin film are characterized by the same reflectivity* p):

(a) p is independent of the film thickness t and is common to *all* members of the family.
(b) The unknown quantities $\ell_0(T)$ and ρ_0 (T) are independent of film thickness t.

As will be discussed below, these assumptions turned out to be at variance with resistivity data analysis carried out using as input the surface roughness measured via independent experiments—hence the validity of resistivity data analysis based upon these two assumptions *and the value of the adjustable parameters published over several decades seems questionable*.

It seems appropriate to mention that there are a number of classical theories of size effects (in the absence of grain boundaries) published in the fifties, sixties, and seventies, where methods to solve BTE were employed to calculate the resistivity of metallic specimens; for completeness, we mention a few of the most relevant. Soffer used boundary conditions similar to those of FS, but proposed instead an angular dependent specularity function $p(\theta) = \exp\left[-((4\pi\delta/\lambda_F)\cos(\theta))^2\right]$, where δ is the rms roughness amplitude, λ_F is the Fermi wave length, and θ is the angle between the electron momentum and the normal to the surface.[15] Other approaches were used to calculate electron motion based upon BTE.[16–20] One innovative scheme was the "kinetic theory" (name proposed by his author),[21,22] where the electron trajectory is followed within the metal specimen employing the method of characteristics,[23] imposing the FS boundary conditions on the external surfaces; such method was later used to compute the magnetoresistance of metallic samples.[24,25]

To complete this brief overview of classical theories (based upon solutions of the BTE), we present below a summary of another semi classical model that carries no adjustable parameters, Calecki's theory.

2. Theory of Calecki

Calecki's model is a classical theory, for it is based upon BTE. The difference between Calecki's approach and that of Fuchs and Sondheimer is that Calecki assumes that the only scattering mechanism that is relevant in the theory is electron-rough surface scattering, and that the rough surfaces limiting the thin film can be approximately described by two parallel flat planes located at $z = 0$ and $z = t$, plus a small perturbation added to describe the deviations of the rough surfaces relative to the two flat planes. Therefore, the electron momentum q_z along z (direction perpendicular to the film) is quantized as a consequence of the confinement of the electron gas between the two parallel surfaces, hence $q_{z,n} = n\pi/t$, with $n = 0, 1, 2,\ldots$ int$(k_F t/\pi)$, where int(q) denotes the integral part of q, and $n = \nu$ becomes the sub band index. Within this framework, electrons can be represented as plane waves along x and y (the coordinate axis parallel to the thin film), so that $\varepsilon(\nu, \mathbf{k}) = \hbar^2/(2m)[k_x^2 + k_y^2 + q_{z,\nu}^2] = \hbar^2/(2m)[k_x^2 + k_y^2 + (\nu\pi/t)^2]$. Calecki then assigns a Fermi distribution function to each sub band, $f_0[\varepsilon(\nu, \mathbf{k})] = 1/[1 + \exp(\varepsilon(\nu, \mathbf{k}) - \varepsilon_F)/k_B T]$, and writes a BTE to describe the changes in $f_0[\varepsilon(\nu, \mathbf{k})]$ associated with each sub band caused by electron-surface scattering.

One representation of the rough surface profile can be obtained using a Gaussian height-height autocorrelation function (ACF), $h^2(x, y) = \delta^2 \exp[-(x^2 + y^2)/\xi^2]$, where (δ, ξ) are the rms surface roughness amplitude and lateral correlation length, respectively.

There are two distinct features of this theory that set it apart from other classical theories of size effects based upon BTE: (a) The theory *contains no adjustable parameters*, for the properties of the rough surfaces limiting the film are described in terms of (δ, ξ) rather than in terms of (adjustable) specularities, and these two quantities (δ, ξ) can be measured routinely employing a STM endowed with atomic resolution. (b) *The theory ignores the electron scattering mechanisms at work in the bulk,* and only describes the effect of transitions between sub bands caused by electron-rough surface scattering. The result is that the conductivity of a thin metallic film can be calculated exactly from

$$\sigma = \sum_{\nu} \frac{n_\nu e^2}{m^*} \sum_{\mu} \langle T(\varepsilon)_{\nu\mu} \rangle_\nu. \tag{5}$$

[Eq. (32) in Ref. 26], where e is the electron charge, m* is the electron effective mass, n_ν is the electron density in sub band ν, T $(\varepsilon)_{\nu\mu}$ is the "collision time" matrix, and the symbol $\langle\psi\rangle_\nu$ stands for the average of the quantity ψ over sub band ν [Eq. (29) in Ref. 26]. To compute the conductivity $\sigma = 1/\rho$, it becomes necessary to calculate numerically the matrix $C(\varepsilon)_{\nu\nu'}$ [Eq. (19) of Ref. 26], which describes electron-surface scattering, given by

$$C(\varepsilon_F)_{\nu\nu'} = \frac{S\pi^2}{4\hbar t^6} \delta^2 \xi^2 \left[\delta_{\nu\nu'} k_\nu^2 \nu^2 \sum_{\mu=1}^{\nu F} \mu^2 I_{\nu\mu}(\xi k_{\nu\mu}) - k_\nu k_{\nu'} \nu^2 \nu'^2 J_{\nu\nu'}(\xi k_{\nu\mu}) \right] \tag{6}$$

with $k_\nu = \sqrt{\left(k_F{}^2 - \left(\frac{\pi\nu}{t}\right)^2\right)}$ [Eq. (59) in Ref. 26], where k_F is the Fermi wave vector; the quantities I and J (appropriate for the case of a Gaussian autocorrelation function) are given by

$$(I)_{\nu\mu} = 2\pi^2 \exp\left[-\frac{1}{4}\xi^2\left(k_\nu{}^2 + k_\mu{}^2\right)\right] I_0\left(\frac{1}{2}\xi^2 k_\nu k_\mu\right), \quad (7)$$

$$(J)_{\nu\mu} = 2\pi^2 \exp\left[-\frac{1}{4}\xi^2\left(k_\nu{}^2 + k_\mu{}^2\right)\right] I_1\left(\frac{1}{2}\xi^2 k_\nu k_\mu\right), \quad (8)$$

which are Equations (3) and (4) of Ref. 27, and I_0 and I_1 are the modified Bessel functions of order zero and 1, respectively.

The resistivity $\rho = (\sigma_0)^{-1}$ induced by electron-surface scattering can be univocally determined from the parameters $(\delta,\ \xi)$, where in this theory, σ_0 is the conductivity coefficient defined by Equation (32) in Ref. 26. However, in order to compare theory and experiment, the non-diagonal matrix $C_{\nu,\nu'}$ given by Eq. (6) must be diagonalized numerically, and the electron scattering mechanisms acting in the bulk must be added as diagonal elements in the "collision time" matrix $T(\varepsilon)_{\nu\mu}$.

3. Including the effect of electron-phonon plus electron-impurity scattering in the formalism of Calecki

To compare theoretical predictions with experimental data using Calecki's theory, electron scattering by phonons and by randomly distributed impurities/point defects must be added to electron-surface scattering. Rather than inverting the matrix C [Equation (6)], we used instead the approach of numerically solving $CX = Y$. This method is significantly faster and reduces considerably the numerical error.

Nevertheless, electron scattering in the bulk does not induce sub band mixing, *for the identity of the electronic states plays no role whatsoever in the scattering processes that take place in the bulk*. Consequently, the corresponding matrix T is diagonal, for it reduces to $T = \tau_{BULK}$, where τ_{BULK} represents the collision time describing electron scattering in the *bulk common to all sub bands*. The matrix T is defined by $C(\varepsilon)T(\varepsilon) = F(\varepsilon)$ [Eq. (22) in Ref. 26]. Matrix $C(\varepsilon)$ depends upon the scattering rates characterizing each electron scattering mechanism. But matrix $F(\varepsilon)$ [defined by Eq. (20) from Ref. 26] is a *diagonal matrix independent of the scattering mechanism*. When two electron scattering mechanisms are present (for example, mechanism A—electron scattering in the bulk, and mechanism B—electron-surface scattering), we have $C_A T_A = C_B T_B = F$; hence, $C_A + C_B = F(T_A{}^{-1} + T_B{}^{-1})$. Since the scattering rates due to electron-surface scattering and electron scattering in the bulk are additive, to compute the matrix C describing both scattering mechanisms acting simultaneously, the product $F(\varepsilon)_{\nu\nu}$ times $1/\tau_{BULK}$ ought to be added to the diagonal elements $C(\varepsilon)_{\nu\nu}$ arising from electron-rough surface scattering.

To determine the temperature dependence of the resistivity at temperatures T, $4\,K < T < 300\,K$, following the procedure outlined above, we computed the collision time corresponding to electron-impurity/point defect scattering at 4 K (Equation (45) of Ref. 26) and added the phonon contribution according to Mathiessen's rule, $1/\tau = 1/\tau_{IMP} + 1/\tau_{EL\text{–}PHON}$, where the first (temperature-independent) term accounts for electron scattering by impurities, and the second (temperature-dependent) term accounts for electron-phonon scattering.[27] The temperature dependence of the resistivity predicted by Calecki's model was computed using the *numerical solution of the transport equations contained in the model, involving no approximations,* incorporating electron-scattering in the bulk in the manner described.

C. Quantum theories of electron-surface scattering

Quantum theories of size effects are theories where the solution of BTE under the boundary conditions invented by Fuchs and Sondheimer is abandoned, and where electron motion is described instead using different formalisms based upon Quantum Mechanics, and where the presence of grain boundaries is entirely ignored (to mention some of them, see Refs. 28–47). The goal of theoretical research performed since the mid-eighties involving quantum theories of size effects has been to build a formalism entirely based upon Quantum Mechanics that would permit the prediction of the increase in resistivity due to electron collisions with the rough surfaces limiting the metallic film—in the absence of grain boundaries—from first principles *without adjustable parameters,* simply from the information contained in the topography characterizing the rough surfaces. Several quantum theories that satisfy this requirement have been published.

1. Theory of Tesanovic, Jaric, and Maekawa (TJM)

These authors considered an electron gas contained within two rough surfaces, and the corrugations on the (x, y) plane are described as small fluctuations superimposed onto two flat planes located at $z = 0$ and $z = t$. The authors used a non-unitary transformation to smooth out the flat surfaces, leading to an effective Hamiltonian. The authors solved the Green's function for this effective Hamiltonian for the case where the confining potential is that of a particle in a box, and consequently, the electron momentum along z (direction perpendicular to the thin film) is quantized. They computed the conductivity using Kubo's formula assuming that the surface roughness profile is well described by a Gaussian of amplitude δ. The result is

$$\frac{\rho}{\rho_0} = \left[\frac{1}{N_C}\sum_{n=1}^{N_c}\left(1 + \frac{\ell}{\ell_{max}}n^2\right)^{-1}\right]^{-1}. \quad (9)$$

[Equation (7) from Ref. 45], where $\ell_{max} = 6\pi(N_C{}^2/k_F{}^2\delta^2)t$, ℓ is the mean free path in the bulk, N_C is the number of occupied sub bands, and k_F is the Fermi wave vector.

2. Theory of Trivedi and Aschroft (TA)

Trivedi and Aschroft studied the same problem that motivated the publication by Tesanovic-Jaric-Maekawa, using also a non-unitary transformation to smooth out the flat surfaces. Following a somewhat different strategy of

calculation, but using the Kubo's linear response theory, they arrived at the following expression for the resistivity [Equation (4.13) in Ref. 47]:

$$\rho = \left[\frac{e^2}{\hbar\pi t}\sum_{n=1}^{N_c}\frac{1-n^2/\kappa^2}{\frac{2N_C+1}{k_F l\kappa}+\left(\frac{\delta}{t}\right)^2\frac{s(N_C)n^2}{3\kappa}}\right]^{-1}, \quad (10)$$

where $\kappa = k_F t/\pi$ and $s(N_C) = (1/2)(1+1/N_C)(2+1/N_C)$.

However, the most relevant quantum theory seems to be the work published by Sheng, Xing and Wang (SXW), for it is the first quantum theory that goes over the classical FS limit, in the sense that it reproduces the results of the FS theory if we ignore the discreteness of the energy levels inherent to the quantum model and replace the sum over the discrete electron states confined in a metallic film (bound by two approximately flat parallel surfaces) by an integral over the solid angle, and if we consider a constant reflectivity rather than the quantum reflectivity furnished by theory.

3. Theory of Sheng, Xing, and Wang (SXW)

The theory of Sheng, Xing, and Wang (SXW)[29] unifies the quantum transport theories then available (TJM and TA), applicable to different special cases, with the classical FS formalism. SXW calculated the Green's function describing an electron gas confined within two (approximately parallel) potential barriers described as randomly rough surfaces. SXW computed the dissipative part of the electron self-energy due to electron scattering by the rough surfaces using Dyson's equation, and proceeded to calculate the conductivity of the film using Kubo's linear response formalism. SXW modeled the surface roughness by a white-noise surface profile, assuming that the height-height autocorrelation function (ACF) that on the average characterizes the rough surface is proportional to a Dirac's delta function, and hence its 2-D Fourier transform is a constant independent of the in-plane momentum of the electron.

The main result obtained by SXW is

$$\frac{\sigma}{\sigma_0} = 1 - \frac{3}{2}\frac{\ell_0}{t}\frac{1}{X_0 N_c}\sum_{n=1}^{N_c} u_n\left(1-u_n^2\right)\frac{\left(1-R(u_n)\right)\left(1-E_d(u_n)\right)}{1-R(u_n)E_d(u_n)}, \quad (11)$$

where $u_n = \frac{q_n}{k_F} = \cos\theta_n = \frac{n\pi}{tk_F}$, $X_0 = \frac{3}{2}\left[1-\frac{1}{3}\left(\frac{N_c}{X_c}\right)^2\left(1+\frac{1}{N_c}\right)\left(1+\frac{1}{2N_c}\right)\right]$, with $X_c = \frac{tk_F}{\pi}, N_c = \mathrm{int}(X_c), E_d(u_n) = \exp\left(-\frac{t}{u_n\ell}\right)$, and

$$R(u_n) = \left[(1-k_F\cos\theta_n Q(k_{||}))/(1+k_F\cos\theta_n Q(k_{||}))\right]^2. \quad (12)$$

Equation (11) is Equation (11) in Ref. 29, and it is the quantum version of Equation (4) in the FS theory. In the quantum version of FS, the integral has been replaced by a sum over the occupied sub bands (the energy levels are determined by the poles of the Green's function describing the electron gas confined between two parallel flat surfaces); each sub band is characterized by q_n, a quantized electron momentum along z [from $n=1$ to $n=N_C=\mathrm{int}\ (tk_F/\pi)$], and the constant reflectivity p that has been replaced by the corresponding quantum reflectivity $R(u_n) = [(1-k_F\cos\theta_n Q(k_{||}))/(1+k_F\cos\theta_n Q(k_{||}))]^2$, Equation (12), which depends on the angle θ_n and depends on the self-energy $Q(k_{||})$ of the electron gas confined within the film. The roughness profile of the surface determines the self-energy $Q(k_{||})$. In the original SXW paper, the self-energy Q is given by Equation (5) of Ref. 29

$$Q(k_{||}) = -\Im m\int\frac{d^2q_{||}}{(2\pi)^2}\langle h^2(q_{||})\rangle\left[VG(q_{||},k_{||})\right], \quad (13)$$

where $\langle h^2(q)\rangle$ represents the average of the 2-D Fourier transform of the height-height autocorrelation function $h^2(q)$ describing the surface roughness, over many realizations of the rough surface, and VG(q, k) describes the 2-D Fourier transform of the product of the confining potential V and the Green's function G.

Since at the time this work was published, no measurement of the height-height autocorrelation function (ACF) describing the surface roughness was available, SXW used the white noise approximation, where the ACF was assumed to be proportional to a Dirac's delta function; hence, its 2-D Fourier transform turns out to be a constant (that may be considered as an adjustable parameter).

4. Quantum version of the Fuchs-Sondheimer model: Modified theory of Sheng, Xing, and Wang (mSXW)

To avoid having, again, *an adjustable parameter in this quantum version of FS theory,* in our group, we investigated this problem theoretically and experimentally. From the point of view of experimental work, we measured with a STM the ACF on a 70 nm gold film deposited on mica to find out a typical value of the relevant parameters (δ, ξ) appropriate for gold films,[28] and then measured the ACF on a family of gold films of different thicknesses evaporated onto mica substrates, as will be discussed below. From the point of view of theory, we removed the limitations imposed by the white noise approximation, simply by computing the self-energy Q given by Equation (13), using the 2-D Fourier transform of a Gaussian ACF. The result is the following:

$$Q_n(k_{||}) = \frac{\xi^2\delta^2}{2t}\pi\exp\left(-\frac{\xi^2}{4}\left(k_{||}^2+k_F^2\right)\right)\times\sum_n\left(\frac{n\pi}{t}\right)^2\exp\left[\left(\frac{n\pi}{t}\right)^2\frac{\xi^2}{4}\right]\times I_0\left(\frac{\xi^2}{2}k_{||}\sqrt{k_F^2-\left(\frac{n\pi}{t}\right)^2}\right), \quad (14)$$

where $k_{||} = (k_x, k_y)$, and I_0 is the modified Bessel function of order zero.[27,28] It seems apparent that, according to the quantum theory, for two thin films to have the same specularity, *the two films must have the same self-energy (14).* The

quantum version of FS theory indicates that this seems extremely unlikely; hence, one of the sweeping simplifying assumption used in the resistivity data analysis based upon the FS theory (the assumption that the specularity p of thin films made out of the same metal—prepared under similar conditions of evaporation—is the same regardless of film thickness) breaks down.

A few comments are in order regarding the comparison of the classical FS model and its quantum version, the mSXW theory: (a) The mSXW theory [Equation (11)] goes over the classical FS model [Equation (4)] in the case of thick films having a large number of quantized states (of order 100 or larger), if the quantum reflectivity [Equation (12)] is replaced by a constant reflectivity p. (b) The mSXW theory contains *no adjustable parameters*, the resistivity of the films is determined by parameters (δ, ξ) which can be routinely measured with an AFM or STM displaying atomic resolution, as discussed in Section IV C 1. (c) In the limit $\ell_0 \to \infty$ the factor (ℓ_0/t) in the RHS of Equation (11) cancels out, so the conductivity of the film (σ) is always smaller than the conductivity of the bulk (σ_0) and energy dissipation arising from electron-rough surface scattering is well accounted for.

5. Determination of the bulk resistivity ρ_0 and bulk mean free path ℓ_0, using as input the surface roughness data (δ, ξ)

At this point, it seems appropriate to ask how the measurements of the parameters (δ, ξ) describing the surface ACF (for example, using a STM endowed with atomic resolution) may be used for comparing theory with experiment *using no adjustable parameters*. The lack of information regarding the bulk conductivity σ_0 and the bulk mean free path ℓ_0 (the conductivity and mean free path that would be observed on each sample *if electron-surface and electron-grain boundary scattering were switched off*) had plagued research on size effects for decades, for the *sweeping assumption had to be made that these parameters are the same for a family of films of different thicknesses prepared under similar experimental conditions.*

We start by noting that the residual resistivity [the temperature independent additive term appearing in the Bloch-Gruneisen theory, Equation (1), describing the resistivity of crystalline metals] depends on the concentration of impurities/point defects present in the crystal, *and these concentrations do depend on the preparation of the crystal*. In the case of metallic interconnects, something similar may be expected to happen. The calculation of the film resistivity at temperature T, $\rho(\mathrm{T})$, predicted by *any* of the theories of size effects faces the severe practical difficulty that the ratio $\rho(\mathrm{T})/\rho_0(\mathrm{T}) = [\sigma(\mathrm{T})/\sigma_0(\mathrm{T})]^{-1} = \mathrm{g}(\delta, \xi, \mathrm{x})$ depends on the parameter $\mathrm{x}(\mathrm{T}) = \ell_0(\mathrm{T})/\mathrm{t}$—where $\mathrm{g}(\delta, \xi, \mathrm{x}) > 1$ is a function (predicted by theory) that describes the *increase in resistivity attributable to electron-surface scattering*. Consequently, to calculate $\rho(\mathrm{T})$, *we need to know $\rho_0(T)$ and $\ell_0(T)$ that characterize the bulk at temperature T for each sample, and these parameters are not known a priori*.

To determine the unknown quantity $\ell_0(4)$, we imposed a condition of self-consistency: That $\ell_0(4)$ must be such that the theoretical prediction (regardless of which theoretical model is employed to describe size effects) coincides with experimental data at 4 K, temperature at which the contribution to the film resistivity arising from electron-phonon scattering is negligible because the phonons are frozen out. We plotted $\rho(4) = \rho_0[\ell_0(4)]\mathrm{g}[\delta, \xi, \mathrm{x}(4)] = \frac{m^* v_F}{nq^2} \frac{g\left(\delta, \xi, x(4) = \frac{\ell_0(4)}{t}\right)}{\ell_0(4)}$ as a function of the bulk mean free path $\ell_0(4)$ at 4 K, for each theory and for each sample, employing the values of (δ, ξ) *measured through independent experiments preformed on each sample*. From the plot we found the value of $\ell_0(4)$ and the corresponding $\rho_0(4)$, that reproduces the residual resistivity $\rho(4)$ measured on each specimen. The results coincide with previous resistivity data analysis following an iteration procedure already published.[48,49] *These values of $\ell_0(4)$ and $\rho_0(4)$ represent the mean free path and resistivity that would be observed at 4 K on each film if electron-rough surface scattering was switched off*. To obtain the temperature dependence of $\ell_0(\mathrm{T})$ and $\rho_0(\mathrm{T})$, we used the procedure described below.

The bulk resistivity $\rho_0(4)$ obtained as indicated allows an estimation of the bulk collision time $\tau_0(4) = \mathrm{m}^*/(\mathrm{nq}^2\rho_0(4))$, as well as the bulk resistivity $\rho_0(\mathrm{T})$ and bulk mean free path $\ell_0(\mathrm{T})$ at $\mathrm{T} > 4$ K. Increasing temperature T adds a statistically independent collision time $\tau(\mathrm{T})_{\text{EL-PHON}}$ due to electron-phonon scattering; *here, we assume that electron-phonon scattering in the thin film is well represented by the data available describing electron-phonon scattering in the crystalline metal*. The validity of this assumption may be questioned, as discussed in Sec. VII B. We computed the average time between collisions in the bulk at temperature $\mathrm{T} > 4$ K using the Bloch-Gruneisen theory following Matthiessen's rule: $1/\tau_0(\mathrm{T}) = 1/\tau_0(4) + 1/\tau(\mathrm{T})_{\text{EL-PHON}}$. We obtained $\tau(\mathrm{T})_{\text{EL-PHON}}$ from the values of the intrinsic resistivity $\rho_0(\mathrm{T})_{\text{EL-PHON}}$ (arising solely from electron-phonon scattering at temperature T) for crystalline gold.[10]

The same method of data analysis was employed to compare resistivity data with the theoretical predictions of the quantum theory of electron-grain boundary scattering presented in Section II E.

6. Quantum theory of resistivity arising from electrons colliding with a rough fractal surface

Another point that seems interesting is that in the nineties, it was suggested that the surface roughness of metallic films could, perhaps, be described as a self-affine fractal. We investigated this proposition both from the theoretical as well as from the experimental point of view. From the theoretical point of view, we computed the conductivity of a metallic film limited by a rough surface such that the 2-D Fourier transform $\mathrm{F}(\mathrm{k}_{||})$ of the height-height ACF corresponding to a self-affine fractal is given by the so called k-correlation model

$$\mathrm{F}\left(\mathrm{k}_{||}\right) = \frac{2\pi\delta^2\xi^2}{\left(1 + A\mathrm{k}_{||}{}^2\xi^2\right)^{1+H}}, \tag{15}$$

where δ is the rms roughness amplitude, ξ is the lateral correlation length, H is the Hausdorff roughness exponent related to d_f (the local fractal dimension), $d_f = 3\text{-}H$, and A is a normalization constant. This form for $F(k_{||})$ was employed in the mSXW model, and the self-energy Q of the electron gas was computed from Equation (13); the result is[50]

$$Q(H, k_{||}) = \frac{\pi\delta^2\xi^2}{t}\sum_{n=1}^{N_c}\left(\frac{n\pi}{t}\right)^2 \frac{F(1+H, 1/2, 1; z)}{\left[1 + A\xi^2\left(k_{||} + q_n\right)^2\right]^{1+H}}, \tag{16}$$

where $q_n = n\pi/t$ and F is the hypergeometric function defined by

$$F(a, b, c; z) = \frac{\Gamma(c)}{\Gamma(b)\Gamma(c-b)}\int_0^1 t^{-\frac{1}{2}}(1-t)^{c-b-1}(1-tz)^{-a}dt,$$
$$\mathrm{Re}(c) > \mathrm{Re}(b) > 0. \tag{17}$$

The calculation of the conductivity of the films proceeds using this self-energy, Equation (16) (appropriate to describe a fractal surface), into Equations (11) and (12).

The experimental verification to answer the question of whether or not the rough surface on a family of gold films evaporated onto mica substrates can be described as a self-affine fractal was published in Ref. 51; the answer is, yes—the roughness of gold films does obey a fractal scaling law.

D. Classical theory of electron-grain boundary scattering

Measurements of the resistivity on thin metallic films of increased purity revealed that as the film thickness shrinks, the resistivity does not obey the FS prediction—no matter what surface reflectivity is used to describe the data—, as pointed out in Ref. 14. However, in many experiments it was found that the increase in resistivity observed in thin films (when compared to the crystalline samples) exceeded what could be expected from the FS theory. Mayadas and Shatzkes (MS) attributed this increase in resistivity to electron scattering by grain boundaries contained in the film; consequently, they developed a theory of resistivity that includes electron scattering by both rough surfaces and by grain boundaries, that is also based upon a solution of BTE.[1] In spite of its severe limitations (that will be discussed below), the MS theory represents a huge step forward, for it can be considered as a recognition that electron-grain boundary scattering may also lead to an increase in resistivity associated with size effects.

1. Theory of Mayadas and Shatzkes (MS)

Mayadas and Shatzkes assumed that the external electric field **E** was oriented along x, and that the grain boundaries were (y, z) planes perpendicular to x. They represented the grain boundaries by a series of delta functions located at x_n having the same strength S_{MS}

$$V(\mathbf{r}) = V(x) = S_{MS}\sum_{N=-N/2}^{N/2}\delta(x - x_n). \tag{18}$$

The Boltzmann equation to be solved is

$$v_z\frac{\partial f_1}{\partial z} + qEv_x\frac{\partial f_0}{\partial \varepsilon} = \frac{f_1}{\tau} + \int P\left(\vec{k}', \vec{k}\right)\left[f_1\left(\vec{k}'\right) - f_1\left(\vec{k}\right)\right]d^3k', \tag{19}$$

which is Equations (4) and (12) in Ref. 1. Here, $P(\vec{k}', \vec{k})$ is the transition probability per unit time, that an electron traveling with momentum $\vec{k}'$ before the scattering event, will come out of it traveling with momentum $\vec{k}$ after the collision, and $f_1(\mathbf{k}) = f(\mathbf{k}) - f_0(\mathbf{k})$, where $f_0(\mathbf{k})$ is the equilibrium Fermi-Dirac electron distribution describing the electron gas in the absence of external fields **E** and **B**, and $f(\mathbf{k})$ is the electron distribution describing the electron gas in the presence of $\mathbf{E} \neq 0$, $\mathbf{B} \neq 0$. To incorporate electron-rough surface scattering taking place at the surfaces that limit the thin film, MS used the boundary conditions invented by Fuchs and Sondheimer; the boundary conditions used by MS are schematically depicted in Fig. 1.

To calculate the transition probability $P(\mathbf{k}, \mathbf{k}')$ induced by electron-grain boundary scattering, the authors computed the square of the matrix elements $|\langle\vec{k}|V|\vec{k}'\rangle|^2$ of potential (18) between plane waves $|\vec{k}\rangle$ and $|\vec{k}'\rangle$, and the result turns out to be proportional to a Kronecker delta $\Delta(k_t - k_t')$ (as a consequence of the fact that the grain boundaries represented in Equation (18) are assumed to be equally spaced), where k_t is the transverse component of k along the (y, z) plane representing the grain boundaries.

This result [Equation (5) in Ref. 1] implies some severe physical restrictions on the model. First, *the authors assume*

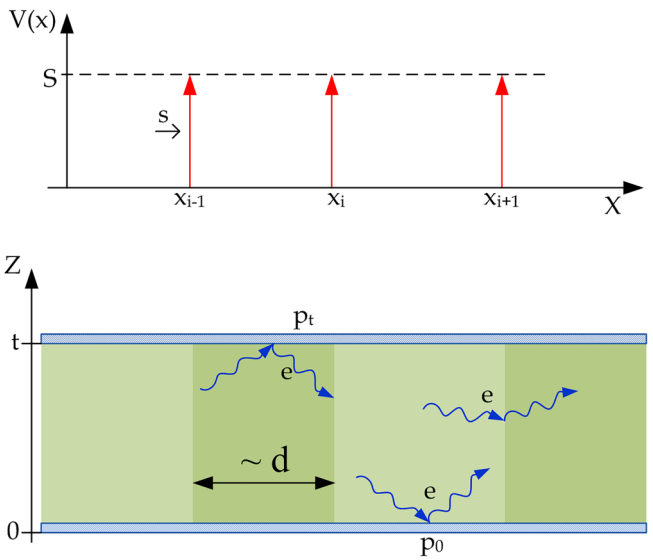

FIG. 1. Schematics of the boundary conditions invented by Fuchs and Sondheimer used by Mayadas and Shatzkes, describing the reflectivity p_0 of the rough surface located at $z = 0$, and the reflectivity p_t of the rough surface located at $z = t$. The shaded areas represent grains exhibiting a different crystalline orientation, separated by an average distance d. The arrows portray the delta function potential representing grain boundaries.

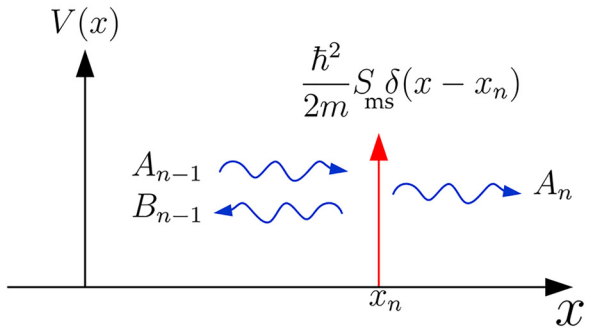

FIG. 2. Schematic representation of a grain boundary located at $x = x_n$, displaying the incident wave A_{n-1}, the reflected wave B_{n-1}, and transmitted wave A_n, respectively, according to the model of Mayadas and Shatzkes.

that the grain boundaries represented by Equation (18) are equally spaced; in the limit $N \to \infty$, this is the well-known Kronig Penney (KP) potential.[52] Second, by computing the transition probability $P(\mathbf{k}, \mathbf{k}')$ using the square of the matrix elements $|\langle \vec{k}|V|\vec{k\prime}\rangle|^2$, the authors use a *first order perturbation theory*, which carries the assumption that *the increase in resistivity arising from electron-surface and from electron-grain boundary scattering are expected to be smaller than or equal to the resistivity observed when grain boundaries and rough surfaces are turned off,* that is, it should be comparable to or smaller than the resistivity arising from electron scattering in the bulk. As will be discussed below, these assumptions turn out to be at variance with experimental results for samples made out of small grains.

The next step in the calculation is to compute the reflection coefficient of a *single grain boundary* located, say, at x_n. The reflection coefficient is $R_n = |B_{n-1}/A_{n-1}|^2$, where B_{n-1} and A_{n-1} represent the amplitude of the plane wave reflected at x_n and incident upon it, respectively, and A_n is the wave transmitted across the grain boundary, as depicted in Fig. 2. Regarding this point, MS assume that *all planes are characterized by the same reflection coefficient R*. To elucidate the implications of this assumption, we chose to describe these electronic states by using the appropriate Bloch waves describing the electron gas in the presence of grain boundaries equally spaced

$$\phi_{n-1}(x) = A_{n-1}\exp(+ik_x x) + B_{n-1}\exp(-ik_x x) \quad \text{valid for } (n-1)d \le x \le nd, \tag{20}$$

$$\phi_n(x) = A_n\exp(+ik_x x) + B_n\exp(-ik_x x) \quad \text{valid for } nd \le x \le (n+1)d, \tag{21}$$

where A_{n-1}, B_{n-1}, A_n, and B_n are complex coefficients describing plane waves that travel from left to right (the A's) and from right to left (the B's). We then impose the following standard boundary conditions for this kind of problem found in an introductory course on Quantum Mechanics:

$$\phi_{n-1}(x = x_n) = \phi_n(x = x_n), \tag{22}$$

$$\left\{\left(\frac{d\phi_n(x)}{dx}\right)_{x=x_n} - \left(\frac{d\phi_{n-1}(x)}{dx}\right)_{x=x_n}\right\} - \frac{2m}{\hbar^2}S_{MS}\phi_n(x = x_n) = 0. \tag{23}$$

These boundary conditions lead to the following relations between the coefficients A, B:

$$A_{n-1}\exp(+ik_x x_n) + B_{n-1}\exp+(-ik_x x_n) = A_n\exp(+ik_x x_n) + B_n\exp(-ik_x x_n), \tag{24}$$

$$A_{n-1}\left[i\frac{2mS_{MS}}{\hbar^2 k_x} + 1\right]\exp(+ik_x x_n) + B_{n-1}\left[i\frac{2mS_{MS}}{\hbar^2 k_x} - 1\right] \times \exp(-ik_x x_n) = A_n\exp(+ik_x x_n) - B_n\exp(-ik_x x_n). \tag{25}$$

In order to compute the reflection coefficient $R_n = |B_{n-1}/A_{n-1}|^2$ characterizing the grain boundary located at x_n, and to arrive at the result of Mayadas and Shatzkes, *we must set $B_n = 0$*. This leads to

$$S_{MS}{}^2 = \left(\frac{\hbar^2 k_x}{m}\right)^2 \frac{R_n}{1 - R_n}, \tag{26}$$

which is used in the calculation of coefficient α in Equation (6c) of Ref. 1, ignoring the fact that S_{MS} depends on k_x, setting instead $k_x = k_F$ and $R_n = R$. This implies that *no further reflection may take place at x_{n+l}*, for having set $B_n = 0$, *then $R_{n+1} = |B_n/A_n|^2$ would be zero.*

The authors continue employing some sort of equivalent collision time τ^* [Equation (7b) in Ref. 1] to describe the effect of electron scattering in the bulk plus electron-grain boundary scattering acting together, assuming the validity of the equivalent of Mathiessen's rule for these two electron scattering mechanisms. To include the effect of electron scattering by the rough surfaces limiting the film, MS employed the boundary conditions invented by FS, with τ replaced by τ^*. As will be shown by in Sec. II E, a quantum mechanical treatment of electron scattering in the bulk plus electron-grain boundary scattering leads to severe violations of Mathiessen's rule; therefore, one of the assumptions underlying MS theory breaks down.

For a film bounded by two different surfaces, the Mayadas and Shatzkes theory yields $\rho/\rho_0 = f(\ell_0(T), d, s, p_0$ and $p_t, R, t)$ (Ref. 53)

$$\left(\frac{\rho_0}{\rho}\right) = \frac{3}{2}\int_{-1}^{1}\frac{\tau^*(u,d,s)}{\tau}u^2 du - \frac{3\ell_0}{4t}\int_0^{2\pi}\int_0^{\pi/2}\left(\frac{\tau^*(\zeta,d,s)}{\tau}\right)^2 \times \frac{\cos^2(\phi)\cos(\theta)\sin^3(\theta)[1 - E(\zeta)]\left[2 - p_0 - p_t + (p_0 + p_t - 2p_0p_t)E(\zeta)\right]}{1 - p_0p_tE(\zeta)^2}d\theta d\phi, \tag{27}$$

$$\text{with } u = \cos(\theta), \quad \zeta = \sin(\theta)\cos(\phi), \quad E(\zeta) = \exp\left(-\frac{t}{v_F \tau^*(\zeta, d, s)\cos(\theta)}\right), \tag{28}$$

$$\text{and} \quad \frac{1}{\tau^*(\varsigma, d, s)} = \frac{1}{\tau} + \frac{\ell_0}{d}\frac{R}{1-R}\frac{1}{\tau\varsigma}\frac{1-\exp\left(-4(\varsigma k_F)^2 s^2\right)}{1-2\exp\left(-2(\varsigma k_F)^2 s^2\right)\cos(2\varsigma k_F d)+\exp\left(-4(\varsigma k_F)^2 s^2\right)}. \tag{29}$$

Here, τ (T) is the average electronic collision time describing electron scattering in the bulk, ℓ_0(T) is the (unknown) electronic mean free path in the bulk at temperature T, d and s are the *average grain diameter and standard deviation characterizing the Gaussian distribution of grain sizes,* respectively. p_0 and p_t are the specularity of the two surfaces limiting the film, R is the reflectivity coefficient characterizing one grain boundary, and k_F is the Fermi wave length. Note that when $R = 0$ and $p_0 = p_t = 1$, Equation (27) yields $\rho = \rho_0$. Hence, ρ(T) represents the resistivity of the film, while ρ_0(T) is the unknown resistivity of the bulk [*the resistivity of a fictitious sample of the same thickness t but without grains (R = 0), carrying the same concentration of impurities/point defects as the thin film, but limited by two atomically flat, perfectly reflecting surfaces, $p_0 = p_t = 1$]. ρ_0(T) represents the resistivity of the thin film, if electron-surface and electron-grain boundary scattering was switched off.*

2. Conceptual difficulties and inconsistencies of the theory of Mayadas and Shatzkes

The first conceptual difficulty of MS theory resides in the inadequate description of the electron wave functions describing the electron gas in the presence of periodically distributed grain boundaries, as plane waves. According to an argument proposed by F. Bloch in the 1930s, if $V(\mathbf{r}+\mathbf{R}) = V(\mathbf{r})$ represents a periodic potential displaying a translational symmetry with periodicity **R**, then Bloch proved that the solutions of the Schrödinger equation can be written in the form of $\phi_{\mathbf{k}}(\mathbf{r}) = \exp(i\mathbf{k}.\mathbf{r})u_k(\mathbf{r})$, *where exp(i**k**.**r**) is a plane wave but modified by the periodic function $u_{\boldsymbol{k}}(\boldsymbol{r}+\boldsymbol{R}) = u_{\boldsymbol{k}}(\boldsymbol{r})$ that displays the periodicity **R** of the lattice regardless of the particular form of V(**r**).*[54,55] The conclusion is that the charge density $|\phi_{\mathbf{k}}(\mathbf{r})|^2 = |u_{\mathbf{k}}(\mathbf{r})|^2 = |u_{\mathbf{k}}(\mathbf{r}+\mathbf{R})|^2$ associated with a Bloch function that represents a solution of the Schrödinger equation, that is, it represents an electron moving in a periodic potential, *is extended throughout the crystal containing periodic grain boundaries, for it exhibits the translational symmetry of the lattice made up of these grain boundaries.*

The correct quantum description of electron states in a crystalline sample containing grain boundaries equally spaced should include the allowed and forbidden states induced by the grain boundary periodicity; the allowed states carry a current across the sample, forbidden states are localized, and hence do not carry any current. Allowed states are not plane waves, they exhibit the periodicity of the lattice of equally spaced grain boundaries. Consequently, *it makes no sense to assume that electrons that occupy some (allowed) energy state in a metallic film made out of periodic grain boundaries will be reflected off at a single (individual) grain boundary.*

The second conceptual difficulty is a consequence of the fact that, for electrons to move through the sample and carry any current, they must traverse one or several grain boundaries and, consequently, the current density in the sample ought to be proportional to the transmission probability T_N that electrons are transmitted through N consecutive grain boundaries. In the theoretical description offered by MS theory, it is assumed that $T_N = 1$. Of all terms contained in the Hamiltonian, Equation (18), electron reflection takes place at ***one*** grain boundary, and the effect of disorder on the position of the grain boundaries relative to the average grain diameter d is severely underestimated, for it depends on $\exp(-x^2)$, where $x = sk_F$, and s is the standard deviation of the Gaussian describing the distribution of grain boundaries. For Cu, Ag, Al, and Au, $k_F \approx 10\,\text{nm}^{-1}$, hence for grains where $d = 10\,\text{nm}$ and $s = 0.1\,d$, $x^2 \approx 100$, so *the effect of disorder in MS theory is severely underestimated and turns out to be completely irrelevant,* for it is of order $\exp(-100)$!!

The third conceptual difficulty arises out of the fact that *grain boundaries are not equally spaced, they are disordered,* and hence, the proper question to ask is: What is the effect of disorder on the eigenfunctions of the KP potential? The answer is known—it led to the Nobel Prize in 1977. Since the work of Anderson and others,[56–58] we know that the solutions of the Schrödinger equation in a randomly varying potential in 1-D are no longer extended but are localized. In the words of Anderson, "…at sufficiently low densities…transport does not take place; the exact wave functions are localized in small regions of space."[56] Moreover, in Chap. 2 of Ref. 58 (p. 7), Thouless states that "…In a weakly disordered one-dimensional potential, all states are localized." The effect of these localized states on the resistance of metallic wires at very low temperatures, in the words of Thouless, leads to "…the resistance should increase exponentially with length instead of linearly."[57]

The fact that MS used plane waves to represent electron states, and the fact that they computed the current density in the sample by assuming that $T_N = 1$ makes it very difficult to include into the calculation the effect of grain boundary disorder that should lead to electronic states that ought to decay exponentially with increasing distance, in what has been termed "weak localization" (weak, for the exponential decay of the electronic states induced by grain boundary disorder is obliterated, once the phase of the electron wave function is randomized, as a result of electron scattering in the bulk).[59]

To correct these severe conceptual difficulties and inconsistencies of MS theory, we outline below a quantum transport theory of electron-grain boundary scattering recently published, where we abandon the Boltzmann Transport Equation and abandon electrons represented by plane waves.

E. Quantum theory of electron-grain boundary scattering

The correct quantum description of electron-grain boundary scattering must start not from the BTE but from the Green's function built out of the solutions of the Schrödinger equation in a 1-D potential representing equally spaced grains

$$V(\mathbf{r}) = V(x) = \sum_{n=-N/2}^{N/2} \left(\frac{\hbar^2 S}{2m}\right) \delta(x - x_n). \tag{30}$$

Note that the strength S that carries each delta function potential is different from that of Eq. (18), where we labelled S_{MS} the strength of each potential of the MS model. Along direction (y, z), the wave functions describing the electron gas should be plane waves, as in MS theory. However, along the direction x, the wave function should be constructed from functions $\varphi_n(x)$ that are solutions of the Schrödinger equation in a 1-D potential represented by Equation (30); so, the electron wave function $\Psi(\mathbf{r})$ reads $\Psi(\mathbf{r}) = f(y,z)\varphi_n(x)$, where $f(y,z) = \exp[i(k_y y + k_z z)]$ are the plane waves used by MS.

1. Solutions of Schrödinger equation for the Krönig-Penney potential

To find the solutions $\varphi_n(x)$ to the Schrödinger equation along x, we impose the following standard boundary conditions:

$$\varphi_{n-1}(x = x_n) = \varphi_n(x = x_n), \tag{31}$$

$$\left\{\left(\frac{d\varphi_n(x)}{dx}\right)_{x=x_n} - \left(\frac{d\varphi_{n-1}(x)}{dx}\right)_{x=x_n}\right\} - S\varphi_n(x = x_n) = 0. \tag{32}$$

We start with

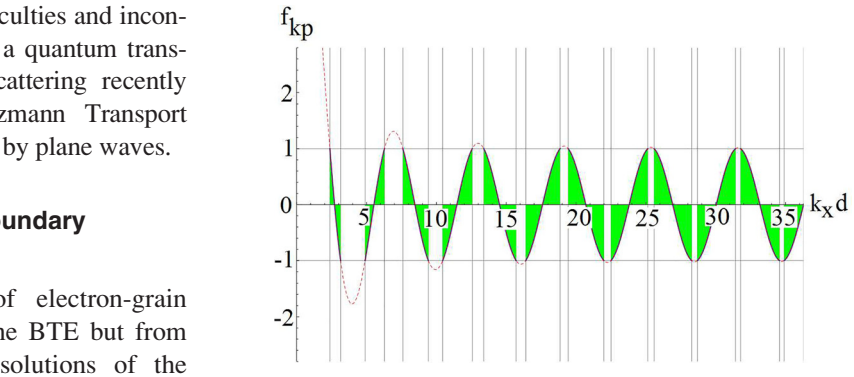

FIG. 3. Allowed and forbidden regions of the KP potential, that occur when d = 3 nm and R = 0.0256. The red line indicates the value of the KP function, Equation (34), the green shadowed areas are allowed bands.

$$\varphi_n(\xi, x) = \exp(in\xi)\sin[k_x(x - (n+1)d)] - \exp[i(n+1)\xi]\sin[k_x(x - nd)], \tag{33}$$

where ξ is the Kronig-Penney parameter. By construction, $\varphi_n(\xi, x)$ already satisfies the condition of continuity, Eq. (31). In order for $\varphi_n(\xi, x)$ to be a solution of the Schrödinger equation in the KP potential (30), it must also satisfy boundary condition (32). To explore this, let

$$f_{KP}(K, u) = \cos(u) + (K/u)\sin(u) \tag{34}$$

be the Kronig-Penney function $f_{KP}(K, u)$ of K and u. Boundary condition (32) leads to

$$\cos(\xi) = \cos(k_x d) + (S/2k_x)\sin(k_x d) = f_{KP}(K = Sd/2, u = k_x d), \tag{35}$$

where ξ is the KP parameter. If ξ is real, then solutions of the Schrödinger equation that extend through the periodic array of grain boundaries exists only for values of k_x such that the right hand side (RHS) of (35) is bounded, $-1 \le RHS \le +1$. The situation is schematically depicted in Fig. 3. The existence of forbidden bands (regions of k_x for which the Schrödinger equation *does not have a solution that extends throughout the periodic array of grain boundaries*) leads to forbidden regions on the Fermi sphere, as illustrated in Fig. 4.

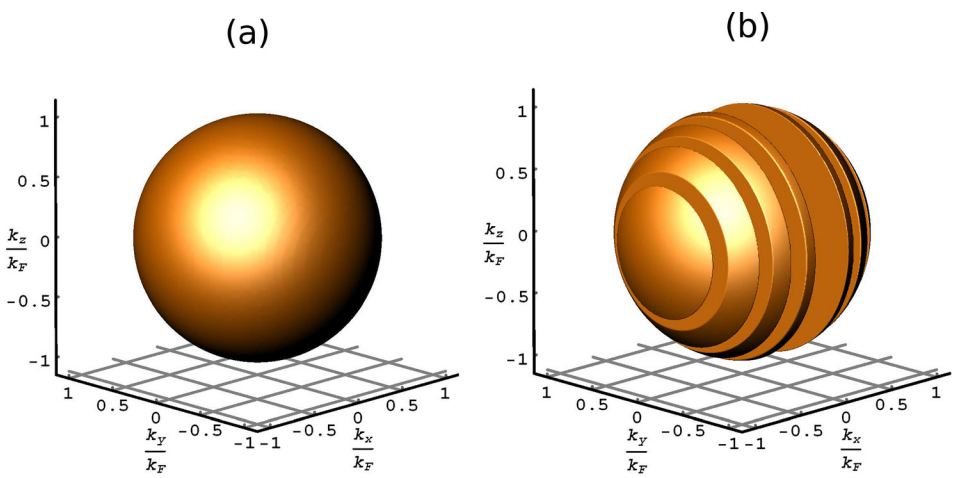

FIG. 4. (a) Fermi sphere for gold. (b) Forbidden KP regions on a gold crystal, when an array of grain boundaries represented by Eq. (30) is added, in the case $k_F = 12.1\ nm^{-1}$ and d = 1 nm.

2. Conductivity of a crystalline sample containing uniform, equally spaced grain boundaries

As shown in Ref. 7, the electrical conductivity of a crystalline sample containing uniform, equally spaced grains can be computed using Kubo's linear response formalism; the result is

$$\sigma = \frac{q^2}{8\pi^2\hbar}\int_0^\infty \frac{I(k)}{|D(k)|^2} T_N(k_x) k_\perp dk_\perp, \tag{36}$$

where $D(k) = k\sin(kd)\sin(\xi)$, with $k = \sqrt{\tilde{k}_F^2 - k_\perp^2}$ (a complex quantity due to the renormalization of k_F to include electron scattering that involves energy dissipation) and $k_x = \sqrt{k_F^2 - k_\perp^2}$. Also

$$I(k) = I_A(k) + I_B(k) + I_C(k) \tag{37}$$

with

$$I_A(k) = \sinh(2\xi_I)\left[\frac{k_R^2}{k_I}\sinh(2k_I d) - \frac{k_I^2}{k_R}\sin(2k_R d)\right] - \sin(2\xi_R)\left[\frac{k_R^2}{k_I}\sin(2k_R d) + \frac{k_I^2}{k_R}\sinh(2k_I d)\right], \tag{38}$$

$$I_B(k) = \frac{1}{d}[\cos(2k_R d) - \cosh(2k_I d)]\left[\frac{k_R^2 - k_I^2}{k_R^2 + k_I^2}\sinh(2\xi_I) + \frac{2k_R k_I}{k_R^2 + k_I^2}\sin(2\xi_R)\right], \tag{39}$$

$$I_C(k) = 4\Im m\left\{\sin(\xi)\left[i\frac{k_R^2}{k_I} + \frac{k_I^2}{k_R}\right]\sin(kd)\right\} + \frac{2}{d}\Im m\left[\frac{k}{k^*}\sin(\xi)\sin(2k^* d)\sin(kd)\right], \tag{40}$$

where the coefficient $T_N(k_x)$ has been included to represent the probability that an electron will be transmitted through N successive grain boundaries perpendicular to x ($T_N = 1$ if all grain boundaries are equally spaced and if the electron occupies an allowed KP band). Here, k* is the complex conjugate of k, whose real and imaginary parts are k_R and k_I, respectively; ξ_R and ξ_I are the real and imaginary parts of the Kronig-Penney parameter ξ. Eq. (36) is the quantum counterpart of the first term in the right hand side of the classical equation (27) considering flat, perfectly reflecting surfaces ($p_0 = p_t = 1$).

The KP function is used with real $u = d\,k_x$ to calculate the allowed KP bands over the domain $-k_F \le k_x \le k_F$ and to project them onto $k_\perp$ using $k_\perp = \sqrt{k_F^2 - k_x^2}$, so that the integral appearing in Eq. (36) is calculated over real domains in $k_\perp$ which correspond to the *allowed KP bands in* k_x.

3. Conductivity of a thin film bounded by two flat surfaces

As shown in Ref. 7, the conductivity of a thin film bounded by flat surfaces that extends from $z = 0$ to $z = t$ but is infinite along x and y, and contains the grains represented by Eq. (30), predicted by the quantum theory, is given by

$$\sigma = \frac{q^2}{8\pi^2\hbar t}\sum_n \int_0^\infty \frac{I(k_n)}{|D(k_n)|^2} T_N(k_x) dk_y, \tag{41}$$

where $k_n = \sqrt{\tilde{k}_F^2 - k_y^2 - \left(\frac{n\pi}{t}\right)^2}$. Again, $T_N(k_x)$ represents the probability that the electron will be transmitted through N successive grain boundaries. $I(k_n)$ is given by Eq. (37), and the values of k_x lie inside the KP bands of allowed states and are such that $k_x^2 + k_y^2 + \left(\frac{n\pi}{t}\right)^2 = k_F^2$. Equation (41) is the quantum counterpart of the classical Eq. (27).

4. Conductivity of a wire of rectangular cross section bounded by flat surfaces

We extend the treatment to a wire bounded by smooth surfaces, of rectangular cross-section of dimensions D_y, D_z such that $0 \le y \le D_y$, $0 \le z \le D_z$ and very long in the x-direction. The effect of grain boundaries is, again, accounted for by means of the series of delta function potentials used by Mayadas and Shatzkes. As shown in Ref. 7, the electrical conductivity is given by

$$\sigma = \frac{q^2}{4\pi\hbar D_y D_z}\sum_{n,m} \frac{I(k_{m,n})}{|D(k_{m,n})|^2} T_N(k_{m,n}), \tag{42}$$

where $k_{m,n} = \sqrt{\tilde{k}_F^2 - \left(\frac{n\pi}{D_y}\right)^2 - \left(\frac{m\pi}{D_z}\right)^2}$.

We point out that the coefficient T_N was misprinted, and it was omitted from Equation (C.6) in Ref. 7. As before, I(k) is given by Equation (37), and the sum is performed only over those values of n and m such that k_x lie inside the KP bands of allowed states and satisfy

$$k_x^2 + \left(\frac{n\pi}{D_y}\right)^2 + \left(\frac{m\pi}{D_z}\right)^2 = k_F^2. \tag{43}$$

Equation (42) is used to estimate the resistivity of Cu nanometric interconnects of rectangular cross section.

5. Effect of disorder

The effect of disorder has not yet been incorporated into the theory. To include it, we consider the wave functions $\Psi_n(x)$ which describe the Bloch states in the case where the grain boundaries are located at $x = x_n$ but *are not equally spaced*. Hence, instead of Equation (33), we write $\Psi_n(x) = A_n \exp(+ik_x x_n) + B_n \exp(-ik_x x_n)$. Imposing boundary conditions (31) and (32) on $\Psi_n(x)$ leads to

$$A_{n-1}\exp(+ik_x x_n) + B_{n-1}\exp(-ik_x x_n) = A_n \exp(+ik_x x_n) + B_n \exp(-ik_x x_n), \tag{44}$$

$$A_{n-1}[1 + i(S/k_x)]\exp(+ik_x x_n) + B_{n-1}[i(S/k_x) - 1]\exp(-ik_x x_n) = A_n \exp(+ik_x x_n) - B_n \exp(-ik_x x_n). \tag{45}$$

Solving for A_n, B_n in terms of A_{n-1}, B_{n-1}, we obtain the 2×2 transfer matrix P_n defined by $\begin{pmatrix} A_n \\ B_n \end{pmatrix} = P_n \begin{pmatrix} A_{n-1} \\ B_{n-1} \end{pmatrix}$, so

$$P_n = \begin{pmatrix} 1 + i\frac{S}{2k_x} & i\frac{S}{2k_x}\exp(-2ik_x x_n) \\ -i\frac{S}{2k_x}\exp(2ik_x x_n) & 1 - i\frac{S}{2k_x} \end{pmatrix}. \quad (46)$$

Note that $\det(P_n) = 1$. In the quantum theory, the reflection coefficient characterizing the grain boundary located at x_n, is $R_n = |B_{n-1}/A_{n-1}|^2$, which leads to $S^2 = 4k_x{}^2\frac{R_n}{1-R_n}$ instead of Eq. (26). In order to make contact with the classical MS theory and to be able to compare the predictions of both models, we followed the procedure of MS and set $k_x = k_F$, $R_n = R$, so

$$S^2 = 4k_F{}^2\frac{R}{1-R}. \quad (47)$$

To describe the effect of disorder, let $x_n = nd + \Delta_n$ indicate the position of the n-th grain boundary, where d is the average grain diameter and Δ_n is a random variable such that $\langle\Delta_n\rangle = 0$ and $\langle\Delta_n{}^2\rangle = s^2$, $\langle\Delta_n\,\Delta_m\rangle = \delta_{m,n}\,\langle\Delta_n{}^2\rangle = s^2\,\delta_{m,n}$ for $1 \le m, n \le N$. Following MS, we assume that Δ_n is a random variable described by a Gaussian probability density $f(\Delta_n)$ with mean cero and standard deviation s^2, $f(\Delta_n) = \frac{1}{\sqrt{2\pi s^2}}\exp\left(-\frac{\Delta_n{}^2}{2s^2}\right)$. We use the simplifying assumption that Δ_n, Δ_m, the fluctuations in the position of the grain boundary located at $x_n = nd$ for grains located at different sites $n \neq m$ are *uncorrelated, and are characterized by the same mean* $\langle\Delta_n\rangle = 0$ *and the same standard deviation* $\langle\Delta_n{}^2\rangle = s^2$. Under these assumptions, we can write the transfer matrix M relating A_N, B_N to A_1, B_1, as $M = P_N \times P_{N\cdot1} \times \cdots \times P_1$; therefore, the statistical average of the 2×2 matrix M is $\langle M\rangle = \langle\prod_{n=1}^{N} P_n\rangle$. Using the statistical independence of the random variables Δ_n, Δ_m, we write $\langle\prod_{n=1}^{N} P_n\rangle = \prod_{n=1}^{N}\langle P_n\rangle$.

Hence, the only element of the 2×2 matrix P_n that involves the random variable Δ_n and an average over an ensemble of all possible realizations of the grain size distribution is $i\frac{S}{2k_x}\exp(-2ik_x x_n)$. Consequently, the statistical average is $\langle i\frac{S}{2k_x}\exp(-2ik_x x_n)\rangle = i\frac{S}{2k_x}\int_{-\infty}^{\infty} f(\Delta_n)\exp[-2ik_x(nd+\Delta_n)]d\Delta_n = i\frac{S}{2k_x}\exp(-2ik_x nd)\exp(-2k_x{}^2 s^2)$.

To compute the transmission coefficient T_N, we write

$$A_N = M_{11}A_1 + M_{12}B_1,$$
$$B_N = M_{21}A_1 + M_{22}B_1$$

and *set* $B_N = 0$ *but only for the N-th grain boundary* $(N > 1)$; therefore, $A_N = (M_{11}M_{22} - M_{12}M_{21})/M_{22} = 1/M_{22}$. Finally, the transmission coefficient is, rigorously, $T_N(k_x) = \langle\frac{1}{|M_{2,2}(N,k_x)|^2}\rangle$.

We used as a simple estimation $T_N(k_x) \approx \frac{1}{\langle|M_{2,2}(N,k_x)|^2\rangle}$.

Within this line of reasoning, Anderson localization plays no role whatsoever. We stumbled on localization induced by electron scattering by successive disordered grain boundaries, after the evaluation of the transfer matrix P_n using the standard rules of Quantum Mechanics described above, and as a result of numerically evaluating $T_N(k_x) = \frac{1}{|M_{2,2}(N,k_x)|^2}$ via matrix multiplication of N matrices for each of the 4 samples analysed in this work, involving $N = 1, 2, 3,$ up to 50 matrices given by Eq. (46). These results forced us to accept localization, and to look for similar phenomena in other branches of Physics. This way we arrived (at the end of this work) to weak Anderson localization.

If N is considered as the total number of grain boundaries between the measuring contacts, then, in our samples, $N \ge 10^5$, which would lead to T of order 10^{-25}. To include the effect of disorder and yet arrive at a realistic estimation of T_N that is consistent with experimental results, we consider $N = 1$ if $\ell < d$, and $N = \mathrm{Int}(\ell/d)$ if $\ell > d$, where Int(z) is the integer part of z, and $\ell(T)$ is the temperature-dependent (unknown) electronic mean free path in the bulk. This approach will lead to *weak Anderson localization*, for after traversing the grains contained in a mean free path, the electron wave function will lose coherence because of electron scattering taking place in the bulk; hence, it does not really become localized. For this reason, we speak of electrons becoming weakly localized, after traversing a set of N (disordered) grain boundaries.[7,59]

Within the theory presented here, the current density is proportional to the probability of transmission $T_N(k_x, R, \ell)$ of an electron traversing N successive grain boundaries. From the argument by Thouless[57] and the work of several researchers working on Anderson localization [56, 58], it is expected that the probability of transmission $T_N(k_x, R, \ell)$ of an electron traversing N successive grain boundaries will behave as $T_N(k_x, R, \ell) \sim \exp[-\ell/L_{loc}(k_x, R)]$, where $L_{loc}(k_x, R)$ is the so called Anderson localization length.

After accepting the fact that such numerical evaluation of $T_N(k_x, R, \ell)$ led to Anderson's localization, we verified that $\ln(T_N)$ is, indeed, proportional to $-\ell$. However, a technical difficulty arises, because of the stepwise variation of $T_N(k_x, R, \ell)$ that necessarily occurs when a grain boundary is added (or subtracted) from the electron trajectory because of an increasing (or decreasing) temperature dependent electron mean free path $\ell(T)$.

6. Estimation of the transmission coefficient T_N

To circumvent the difficulty arising from the stepwise variation of $T_N(k_x, R, \ell)$ that necessarily occurs when a grain boundary is added (or subtracted) from the electron trajectory along a mean free path in the bulk, and to retrieve the fundamental underlying physics, we numerically computed T_N over a grid of values of (k_x, R) involving (100×9) data points for each sample, using for t, d, and s the values *measured on each sample* listed on Table I, and adjusted a smooth analytic function of (k_x, R) to the resulting T_N numerical data, seeking agreement to 7 significant figures in the neighbourhood of $k_x \approx 0.9\,k_F$ and $R \approx 0.1$, which (as will be seen below) is the region that contributes the most to the conductivity of the samples.

In order to assess how robust the method employed to calculate T_N really is, and how reliable is the analytical representation of $T_N(k_x, R)$, we decided to implement a

TABLE I. Morphological parameters for samples S1, S2, S7, and S8. t: film thickness; d and s: mean diameter and standard deviation of a Gaussian distribution of grains (describing the histogram of over 500 grains per sample); δ and ξ: rms roughness amplitude and lateral correlation length describing a Gaussian roughness profile. ℓ_{IMP}: mean free path (attributable to impurity scattering); R: grain boundary reflectivity, according to the MS model with $p_t = 0$ and $p_0 = 1$. Parameters t, d, s, R, and ℓ_{IMP}: (the latter two appropriate for MS model). Rightmost three columns ℓ_{IMP}: mean free path; R: grain boundary reflectivity; L_{loc}: Anderson localization length, needed to describe the resistivity according to the quantum model. Data taken from Table I of Ref. 7 with permission.

						Classical MS		Quantum		
							R			
Sample	t (nm)	d (nm)	s (nm)	δ (nm)	ξ (nm)	ℓ_{IMP} (nm)	$p_t = 0$ $p_0 = 1$	ℓ_{IMP} (nm)	R	L_{LOC} (nm)
S1	49	11.1	5.3	1.3	8.9	3000	0.41	36	0.1127	106
S2	109	12.4	5.3	1.3	7.3	3000	0.43	41	0.1013	109
S7	54	106	43	3.1	58.4	3000	0.28	137	0.0116	19 400
S8	96	159	41	4.1	68.2	3000	0.22	295	0.0192	12 700

numerical simulation of T_N according to the following procedure:

(i) Given the parameters d, s describing each sample S1, S2, S7, and S8 (from Table I), and given a value of ℓ, an array of random $x_n = (x_1, x_2, \ldots, x_N)$ grain boundaries was generated with $n = 1, 2, \ldots N = \text{int}(\ell/d)$, according to a Gaussian random distribution characterized by the parameters appropriate to describe each sample.

(ii) The randomly numerically generated array of x_n grain boundaries was ordered from the smallest to the largest, such that $x_{0n} = (x_{01}, x_{02}, \ldots, x_{0N})$.

(iii) The transfer matrix P_n was evaluated for each grain boundary, according to Equation (46), with $k_x = 0.9\ k_F$, $R = 0.10$, with S calculated from Eq. (47).

(iv) The transmission coefficient T_{si} for this simulated set of grain boundaries was evaluated as $T_{Si} = \frac{1}{|M_{2,2}|^2} = \frac{1}{|(P_N \times P_{N-1} \times \cdots \times P_1)_{2,2}|^2}$.

(v) The average transmission coefficient was calculated as $\langle T_{Si} \rangle = \frac{1}{N_S} \sum_{n=1}^{N_S} T_{Si}$, where N_S is the number of simulations (Si). We found that 2000 numerical simulations yielded an average transmission coefficient T_{si} with a standard deviation of about 0.5%.

After performing such numerical simulations we compared the results displayed in Fig. 5 for samples S1 and S2. The same comparison was performed for samples S7 and S8 (not shown). We conclude that the analytical estimation of T_N appears to rest on solid ground.

7. Contribution to the resistivity of a thin film arising from energy dissipation involved in electron-rough surface scattering

In this section, we address the issue of how to compute the contribution to the resistivity of a thin film arising from electron-rough surface scattering employing Kubo's formalism. Within the formalism used in Refs. 28 and 29, the wave functions describing the electron gas that extends indefinitely along x and y, but is confined by two rough surfaces at $z = 0$ and $z = t$, is

$$\varphi^-(z) = \exp(-ik_z z) - A_0 \exp(ik_z z),$$
$$\varphi^+(z) = \exp(+ik_z z) - A_t \exp(2ik_z t - ik_z z), \quad (48)$$

where $\varphi^-(z)$ represents the wave function propagating along $-z$, $\varphi^+(z)$ represents the wave function propagating along $+z$, while A_0 and A_t represent the amplitude of the wave functions reflected by the rough surfaces located at $z = 0$ and $z = t$, respectively. In the case of these gold films, we set $A_0 = 1$, since AFM reveals that the mica surface is flat in regions whose lateral dimensions are of the order of a few hundred nm. Within the quantum formalism of Refs. 28 and 29, A_t is given by

$$A_t = \frac{1 - k_z Q_n(k_{||})}{1 + k_z Q_n(k_{||})} = \exp(2i\delta_t), \quad (49)$$

where $Q_n(k_{||})$ is given by Eq. (14), and we have introduced the phase shift δ_t for convenience.

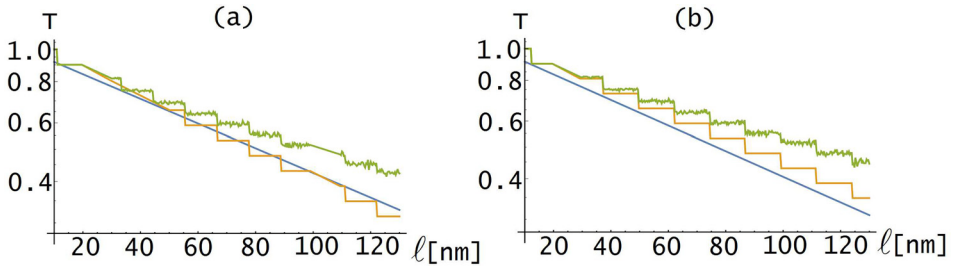

FIG. 5. (a) Transmission coefficient T_N computed using the parameters (d, s) appropriate to describe sample S1 plotted as a function of electron mean free path ℓ. In orange, the result of matrix multiplication evaluated at $k_x = 0.9\ k_F$ in Equation (46) and $R = 0.1$; in green the results of the numerical simulations; and in blue the analytic representation of T_N. (b) Transmission coefficient T_N computed using the parameters (d, s) appropriate to describe sample S2 listed in Table I.

Equation (49) for A_t is consistent with the quantum reflectivity, Equation (12), in the mSXW model. Then, the one-dimensional Green's function is

$$g(k_z; z, z') = \frac{\sin(k_z z)\sin\left[k_z(z'-t)-\delta_t\right]}{k_z \sin(k_z t+\delta_t)} \quad \text{if } z < z', \quad (50)$$

$$g(k_z; z, z') = \frac{\sin(k_z z')\sin[k_z(z-t)-\delta_t]}{k_z \sin(k_z t+\delta_t)} \quad \text{if } z > z'. \quad (51)$$

The energy level of the electron gas is given by the wave vectors $k_{z,n}$ associated with the poles of this Green's function. These poles and the corresponding wave vectors $k_{z,n}$ are obtained by solving Eq. (49) using the corresponding phase shifts δ_t

$$k_{z,n}t = n\pi - \frac{1}{2i}\ln\frac{1-k_{z,n}Q_n\left(k_{||,n}\right)}{1+k_{z,n}Q_n\left(k_{||,n}\right)}. \quad (52)$$

If $\delta_t = 0$, then the Green's function describing the flat surface has poles at $k_{z,n}(\delta_t = 0) = n\pi/t$, where $1 \le n \le \mathrm{Int}(tk_F/\pi)$, which describe the energy levels of the sub bands of the electron gas confined between two parallel flat surfaces.

To determine the complex poles $k_{z,n}$ satisfying Eq. (52) induced by the presence of the rough surface on samples S1, S2, S7, and S8, we computed Q_n according to Equation (14) using the parameters $(\delta,\ \xi)$ listed in Table I for each sample, and used as a first approximation (to compute Q_n), the value $k_{||,n} = \sqrt{k_F{}^2 - \left(\frac{n\pi}{t}\right)^2}$. The transcendental equation (52) was solved numerically for the complex $k_{z,n}$ using a Newton-Rapson method until a precision of 10 digits was obtained for each sub band $1 \le n \le \mathrm{Int}(tk_F/\pi)$.

To include the contribution to the resistivity arising from dissipation caused by electron scattering by the rough surface, the values of $k_{z,n}$ determined numerically were used to shift the Fermi sphere adding an imaginary part to the wave vector k_z. The complex numerical solution of Eq. (52) was employed to compute the corrected values of $k_n = \sqrt{\tilde{k}_F{}^2 - k_{z,n}{}^2 - k_y{}^2}$ for each sub band before performing the integration on Eq. (41). The method to calculate the conductivity over the allowed KP bands on k_x, and of shifting the Fermi sphere by adding an imaginary wave vector to compute the energy dissipation induced by electron scattering with the external rough surface, is schematically illustrated in Fig. 6.

III. SIZE EFFECTS IN THE PRESENCE OF A MAGNETIC FIELD

In this section, we review some experimental manifestations of size effects regarding charge transport measured in the presence of the magnetic field. A detailed discussion of the resistivity originating from size effects measured in the *absence* of the magnetic field, and of the predictive power of different theories of size effects in the absence of grains, is deferred to Secs. IV A, IV B and IV C.

The presence of an electric field **E** and a magnetic field **B** on a nonmagnetic metallic sample results in the Lorentz force acting upon the charge carriers, such that the electron gas acquires a drift velocity which is proportional to **E** and to **E** × **B**

$$\langle \mathbf{v} \rangle = \mu_D \mathbf{E} + \mu_D \mu_H \mathbf{E} \times \mathbf{B}. \quad (53)$$

Here, μ_D is the drift mobility and μ_H is the Hall mobility. In the particular case where $\mathbf{E} = (E_x, E_y, 0)$ and $\mathbf{B} = (0, 0, B)$, we have $\langle \mathbf{v} \rangle = (\langle V_x \rangle, \langle v_y \rangle, 0) = \mu_D(E_x + \mu_H E_y B, E_y - \mu_H E_x B, 0)$. The Hall field is the field E_y needed to cancel out the transverse component of the drift velocity induced by the magnetic field, so that $\langle v_y \rangle = 0$, it is given by $E_H = \mu_H E_x B$. The Hall tangent is defined by the ratio $\tan(\theta_H) = E_H/E_x = \mu_H B$; hence (assuming B is small enough such that μ_H is a constant independent of B), $\mu_H = \frac{\partial(\tan(\theta_H))}{\partial B}$. The conductivity σ of a homogeneous nonmagnetic crystalline solid having one carrier (in the absence of magnetic field) is given by $\sigma = nq\mu_D$, where q is the charge of the carrier and n is the carrier density.

A. Hall voltage

The experimental set up where an external magnetic field **B** is applied orthogonal to the plane of a thin film giving rise to the Hall voltage is schematically depicted in Figure 7. The

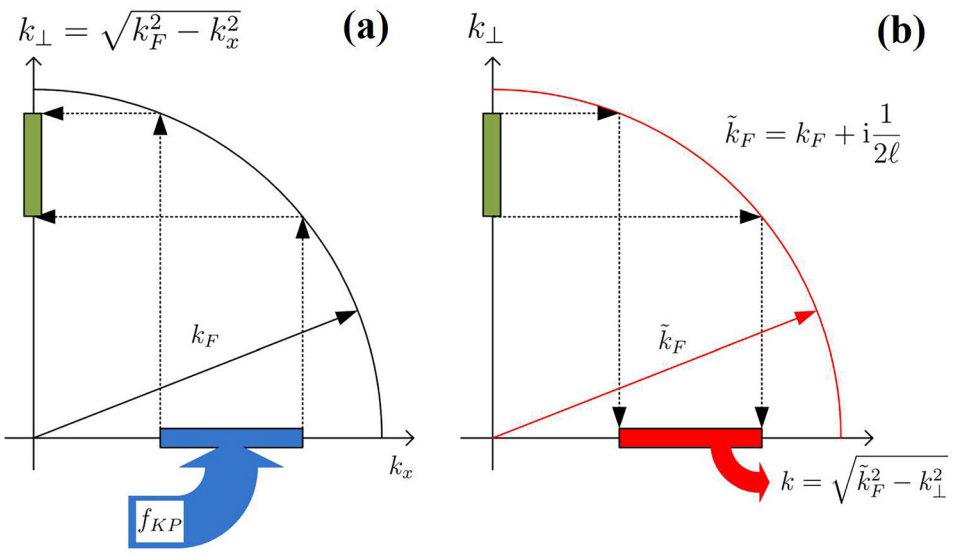

FIG. 6. (a) Projection of the allowed KP bands onto $k_\perp = \sqrt{k_F{}^2 - k_x{}^2}$. Allowed bands of the Kronig Penney function f_{KP} [Equation (34)] along k_x represented in blue; in green the allowed regions in $k_\perp$ the magnitude of $\mathbf{k}_\perp = k_y\mathbf{y} + k_z\mathbf{z}$. (b) Inclusion of a complex part on the Fermi wave vector to account for energy dissipation induced by electron-impurity/point defect scattering and/or electron-rough surface scattering.

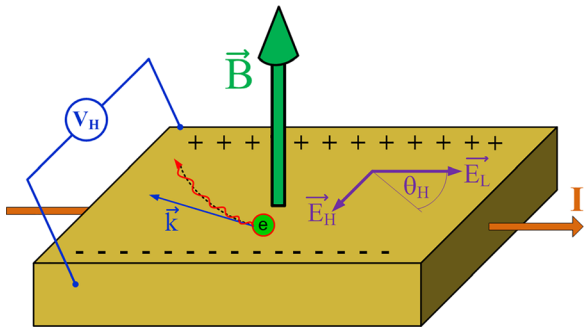

FIG. 7. Experimental set up used to measure the Hall effect, indicating the modification of the electron trajectory between scattering events induced by the magnetic field B that gives rise to the Hall voltage V_H.

presence of the magnetic field **B** orthogonal to the plane of the film induces a curvature on an otherwise straight line electron trajectory that would take place between two scattering events (that would occur in the absence of B), as illustrated in Figure 7. Measuring the Hall voltage V_H in steady state allows the experimental determination of the Hall tangent $\tan(\theta_H) = E_H/E_L$, where $E_H = V_H/w$, where w is the width of the specimen, E_H is the transverse electric field necessary to cancel out the transverse voltage, and E_L is the longitudinal electric field applied to the sample.

The effect of the dimensions of the sample on the Hall voltage and on the magnetoresistance has been recently reported.[60–66] Of these transport coefficients, measuring size effects on the Hall voltage helps elucidating the nature of the microscopic electron scattering mechanisms at work, as will be shown below.

B. Hall tangent and Hall mobility

In a homogeneous crystalline solid, the Hall tangent and the Hall mobility turn out to be independent of the size of the sample, for the *distance traveled by electrons between scattering events* (and hence *the curvature of the electron trajectory induced by the magnetic field) depends only on the nature of the microscopic electron scattering mechanisms at work and does not depend on the boundaries limiting electron motion*; therefore, such distance is independent of whether the sample is, say, a $1\,\mu m \times 1\,\mu m \times 10\,\mu m$ or $10\,\mu m \times 10\,\mu m \times 100\,\mu m$ specimen.

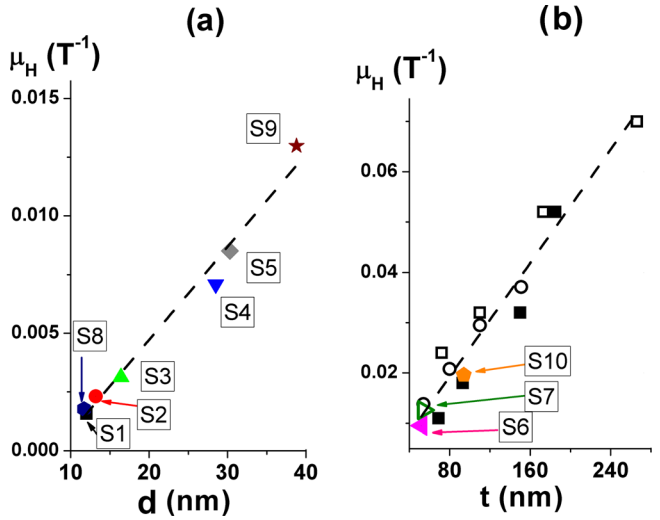

FIG. 9. Dependence of the Hall mobility $\mu_H(4)$ on (a) the average grain diameter d; and (b) on film thickness t. Dashed lines represent the result of a linear regression. Samples S1–S10 identified as in Fig. 8. Data taken from Fig. 2 of Ref. 65.

In thin gold films, this is not the case; the size of the Hall tangent and of the Hall mobility turns out to depend on the size—on the morphology—of the samples. The Hall tangent measured at 4 K in a family of gold films evaporated onto mica substrates, having a thickness of approximately 50 nm and 100 nm, made out of grains whose diameter varies approximately between $10\,nm < d < 150\,nm$, is illustrated in Figure 8. The Hall mobility (determined as $\frac{\partial(\tan(\theta_H))}{\partial B}$) is plotted in Figure 9. The temperature dependence of the Hall mobility measured in samples made out of grains having a different diameter d is displayed in Fig. 10.

The simplest phenomenological interpretation (according to Drude's model) is that the Hall mobility is given by $\mu_H = q\tau_{phen}/m$ (where m is the electron mass and τ_{phen} is the phenomenological average time between collisions). The results displayed in Fig. 10 prove, experimentally, that when the films are made out of small grains such that $d < \ell(4)$,

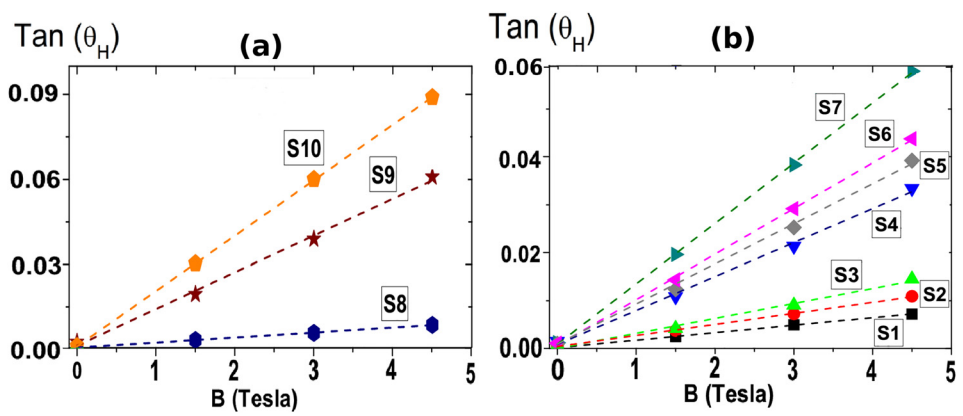

FIG. 8. Dependence of the Hall tangent $\tan(\theta_H) = E_H/E_L$ (E_H: Hall field, E_L: Longitudinal field) on the strength of the magnetic field B, for different samples. (a) Samples approximately 100 nm thick (S8: t = 96 nm, D = 11.7 nm; S9: t = 97 nm, D = 38.8 nm; S10: t = 94 nm, and D = 174 nm). (b) samples approximately 50 nm thick (S1: t = 49 nm, D = 12.0 nm; S2: t = 48 nm, D = 13.2 nm; S3: t = 47 nm, D = 16.4 nm; S4: t = 57 nm, D = 28.5 nm; S5: t = 47 nm, D = 30.3 nm; S6: t = 52 nm, D = 108 nm; S7: t = 54 nm, and D = 110 nm). Dashed lines represent the linear regression. Data taken from Fig. 1 of Ref. 65.

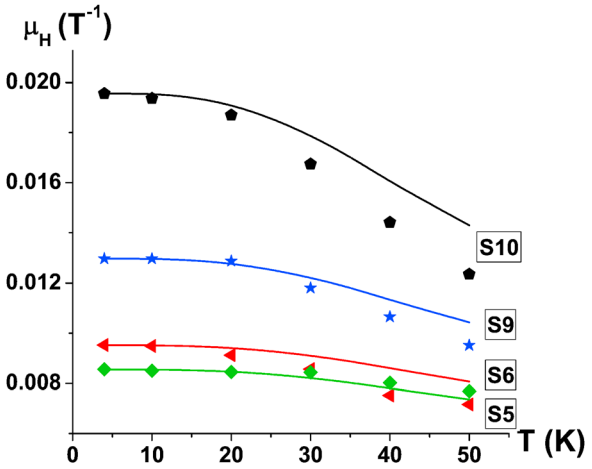

FIG. 10. Temperature dependence of the Hall mobility $\mu_H(T)$ in samples S5 (t = 47 nm, D = 30.3 nm), S6 (t = 52 nm, D = 108 nm), S9 (t = 97 nm, D = 38.8 nm), and S10 (t = 94 nm, D = 174 nm). Solid lines represent the temperature dependence predicted by the additivity of the scattering rates, $\mu_H(T) = \mu_H(4)/[1 + \tau_H(4)/\tau_{PH}(T)]$. Data taken from Fig. 3 of Ref. 65.

τ_{phen} (the phenomenological average time between collisions) depends linearly on the grain diameter d, regardless of the thickness t of the films; *this can be considered the finger print of electron-grain boundary scattering being the dominant electron scattering mechanism controlling charge transport and the resistivity at 4 K*. On the contrary, when the films are made out of columnar grains (extending from top to bottom) such that d > t, then the Hall mobility data prove that τ_{phen} depends linearly on the film thickness t; *this can be considered the finger print of electron-rough surface scattering being the dominant electron scattering mechanism controlling charge transport and the resistivity at 4 K*.

C. Magnetoresistance

The presence of a magnetic field has been observed to induce a change in resistivity in crystalline solids, which is well documented in Ref. 67. Ziman has shown that, based upon the solution of BTE within the relaxation time approximation, a metallic crystal having a perfectly spherical Fermi surface should exhibit no magnetoresistance, because of symmetry (Ref. 68, Chap. 12).

Consequently, measuring the magnetoresistance in thin metallic (nonmagnetic) films and using existing theories of magnetomorphic effects to interpret the data as arising from size effects demands especial care, for the observed magnetoresistance signal could arise from the (often) nontrivial electronic structure of the Fermi surface, from its departures from a perfect sphere on the bulk metal, rather than from size effects.[67] Perhaps one easy way to confirm that the magnetoresistance signal is, indeed, due to size effects (as opposed to departures of the Fermi surface form a perfect sphere in the bulk metal) is to perform the measurement in metal films made out of columnar grains, for which we know that the Hall mobility increases linearly with film thickness; hence, we know that the magnetoresistance arises, indeed, from electron rough surface scattering.

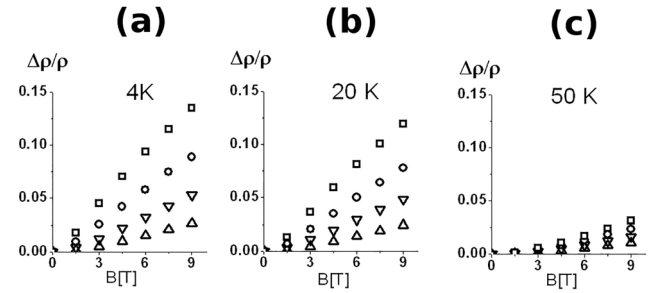

FIG. 11. Dependence of the longitudinal magnetoresistance on the magnetic field B, at different temperatures: (a) 4 K, (b) 20 K, and (c) 50 K, indicated in the figure. Squares: film 266 nm. Circles: film 173 nm. Inverted triangles: film 110 nm. Triangles: film 72 nm. Data taken from Fig. 1 of Ref. 62.

In Figure 11, we plot the longitudinal magnetoresistance $\Delta\rho/\rho = \frac{\rho(B,T)-\rho(0,T)}{\rho(0,T)}$ measured at temperature T in a family of gold films made out of columnar grains, with the electric field **E** oriented parallel to the magnetic field **B**.[62] In Figure 12, we plot the transverse magnetoresistance $\Delta\rho/\rho$ measured in a family of gold films made out of columnar grains, with the magnetic field **B** oriented perpendicular to the plane of the film.[61] In Figure 13, we display the transverse magnetoresistance $\Delta\rho/\rho$ measured in a family of gold films made out of columnar grains, with the magnetic field **B** contained within the plane of the film but oriented perpendicular to the electric field **E**.[63] The data displayed in these figures prove that the value of the magnetoresistance and its dependence on the magnetic field strength does depend on the film thickness, and in all of these samples, the Hall mobility depends linearly on film thickness; hence, the magnetoresistance

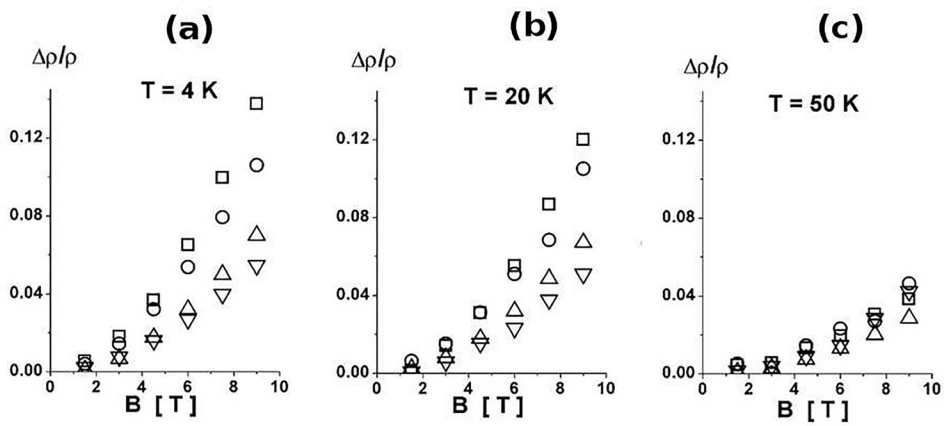

FIG. 12. Dependence of the transverse magnetoresistance on the magnetic field B (B oriented perpendicular to the surface of the film) at different temperatures: (a) 4 K, (b) 20 K, (c) 50 K, indicated in the figure. Squares: film 185 nm. Circles: film 150 nm. Triangles: film 93 nm. Inverted triangles: film 69 nm. Data taken from Ref. 61 with permission.

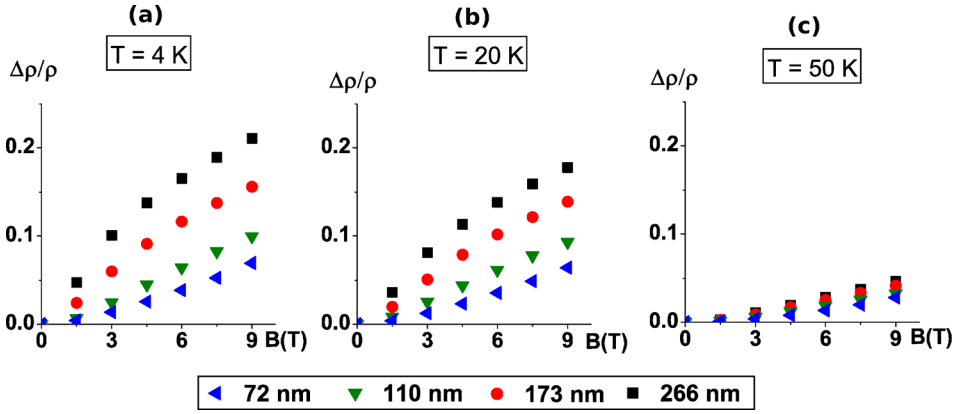

FIG. 13. Magnetic field dependence of the transverse magnetoresistance with the magnetic field **B** oriented perpendicular to the electric field **E**, both (**E**, **B**) contained within the plane of the film, at different temperatures: (a) 4 K, (b) 20 K, and (c) 50 K. Temperature and thickness indicated in the figure. Data taken from Fig. 2 of Ref. 63 with permission.

signal displayed in Figs. 11–13 arises, indeed, from electron-rough surface scattering. The transverse magnetoresistance (measured with the magnetic field **B** contained within the plane of the film but oriented perpendicular to the electric field **E**) is about twice as large as the transverse magnetoresistance measured with **B** orthogonal to the plane of the film, and is about twice as large as the longitudinal magnetoresistance. The theoretical explanation of size effects involving the magnetoresistance data remains open.

IV. RESISTIVITY DATA AND PREDICTIONS OF THEORIES OF ELECTRON-SURFACE SCATTERING (IN THE ABSENCE OF GRAINS)

We begin the discussion regarding the predicting power of theories of size effects and experimental resistivity data in samples where grain boundary scattering can be neglected, for the samples are made out of columnar grains extending from top to bottom, and the Hall mobility μ_H turns out to be proportional to the film thickness t. The discussion of the predicting power of theories where electron-grain boundary scattering plays a significant role is deferred to Sec. V A.

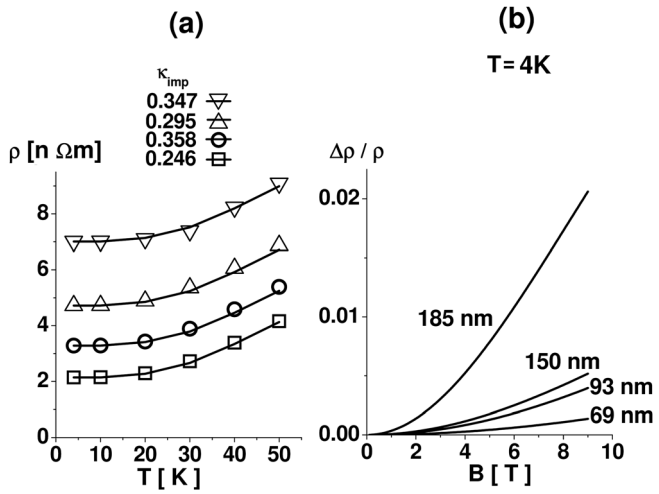

FIG. 14. (a) Temperature dependence of the resistivity for films of different thickness. Squares: film with t = 185 nm; circles t = 150 nm; triangles t = 93 m; and inverted triangles t = 69 nm. Solid line: prediction of Fuchs-Sondheimer theory, with $p_0 = 1$ and $p_t = 0$. The term $\ell_0(4)$ was adjusted to describe $\rho(4)$ for each sample; the corresponding value of $\kappa_{imp} = t/\ell_0(4)$ (at 4 K) is indicated in the figure. (b) Magnetic field dependence of the transverse magnetoresistance with the magnetic field B oriented perpendicular to the surface of the films, predicted by the Fuchs-Sondheimer theory. Data taken from Fig. 3 of Ref. 61 with permission.

A. Predictive power of the Fuchs-Sondheimer theory

For completeness, we display the experimental results and classical theoretical predictions of FS theory in Figure 14. Adjusting $\ell_0(4)$, the mean free path attributable to electron-impurity scattering on each sample at 4 K, the FS theory predicts fairly well the temperature dependent resistivity of thin gold films, but [as displayed in Fig. 14(b)] it predicts a transverse magnetoresistance measured on the same samples, which is *one order of magnitude smaller than observed*.

In order to abandon the comparison between resistivity data and theoretical predictions based upon parameter fitting that has been used for decades, we performed simultaneous measurements of the temperature dependent resistivity at temperature T, $4\,K < T < 50\,K$, as well as the temperature dependence of the magnetoresistance, in thin gold films evaporated onto mica substrates made out of columnar grains. The surface roughness of each sample was measured with a STM endowed with atomic resolution.

B. Predictive power of Calecki's theory

The experimental results and classical theoretical predictions of Calecki's theory are displayed in Figure 15.

The resistivity predicted using the relaxation time τ [Equation (64) from Ref. 26] deduced by the author in the limit of small correlation lengths ($k\xi < 1$) turns out to be two orders of magnitude larger than observed, as displayed in Fig. 15(a). This is not surprising, for the limit of small correlation lengths $k\xi < 1$ does not apply to gold, for which $k\xi > 100$. If we drop the small correlation length approximation employed by Calecki, and use instead the numerical solution of the equations contained in the model, then an average collision time can be found that describes fairly well the temperature dependent resistivity, as displayed in Fig. 15(b), but then the predicted transverse magnetoresistance turns out to be several orders of magnitude smaller than observed. The reason is that, after numerically diagonalizing the matrix C [Equation (6)] to incorporate the effect of electron scattering in the bulk as diagonal elements in the "collision time matrix T," the diagonal elements of T representing the effect of electron scattering in the bulk turn out to be orders of magnitude larger than the off diagonal

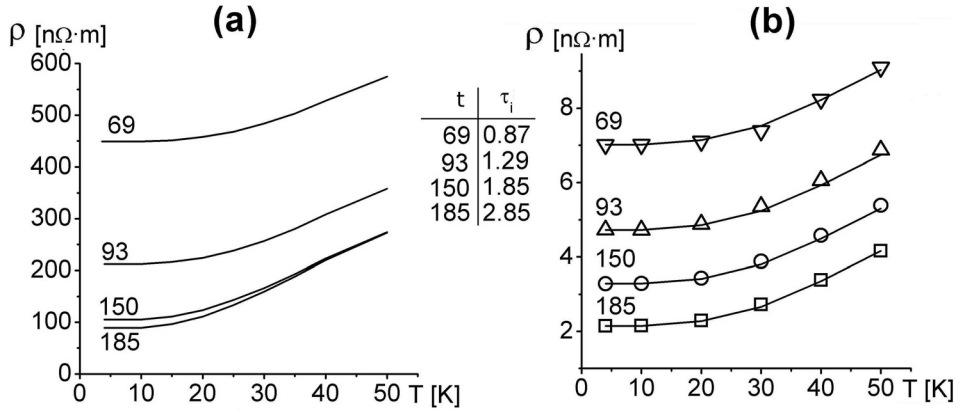

FIG. 15. (a) Temperature dependence of the resistivity predicted by Calecki's theory using the sub band relaxation time given by Equation (1) from Ref. 27. (b) Temperature dependence of the resistivity measured on different films: Squares, film 185 nm; circles: film 150 nm; triangles: film 93 nm; and inverted triangles: film 69 nm. Solid line represents the resistivity predicted on the basis of the numerical solution of the transport equations contained in Calecki's theory. The collision time τ_i (indicated in the figure in units of 10^{-13} s) have been adjusted to describe $\rho(4)$ observed on each sample. Data taken from Fig. 1 of Ref. 27.

elements which represent sub band mixing induced by electron-rough surface scattering.

C. Predictive power of the quantum transport theories

Before addressing the predictive power of quantum theories described in Section II C, we discuss briefly certain aspects which are common to all of them.

1. Determination of the height-height autocorrelation function from precision measurements of the surface topography employing a STM

The quantum theories described in Section II C all assume that the topography of the rough surface (ignoring grain boundaries) is well described by a Gaussian autocorrelation function. This assumption may be considered as a manifestation of the Central Limit Theorem applied to the random sampling of the surface roughness over many realizations of the latter, but remains nonetheless an ad-hoc assumption that had not been tested experimentally until recently. As discussed in detail in Ref. 69, precision measurements of the surface roughness (within one grain) start from the verification that the STM tip exhibits, indeed, atomic resolution running over a sample of Highly Oriented Pyrolitic Graphite (HOPG). After such verification, measurements of the surface topography are performed over a scale of 10 nm × 10 nm containing 256 × 256 pixels each. It seems interesting to note that although the autocorrelation function corresponding to each individual STM image (recorded at random locations of the sample within one grain) does not display the cylindrical symmetry along z (direction perpendicular to the surface of the film) assumed in quantum theories of size effects, it is sufficient to compute an average over 12 or more autocorrelation functions from STM images recorded at random locations of the sample, to restore the assumed cylindrical symmetry; the averaging process leads to an experimental autocorrelation function comprising over 10 000 data points. The remarkable result is that fitting a Gaussian $h(x, y) = \delta^2 \exp[-(x^2 + y^2)/\xi^2]$ to this huge set of experimental data points leads to a quality of the fit (measured through the statistical parameter χ^2/ν) which is of order 1 or smaller, as displayed in Table II; *this can be considered the first experimental verification of the validity of the Central Limit Theorem assumed in quantum theories of size effects*. The details of the measurement can be found in Ref. 69.

2. Interference between electron scattering in the bulk and electron-surface scattering, and violations of Mathiessen's rule

Another feature that is common to the quantum transport theories described in Section II C is quantum interference between electron scattering in the bulk and electron-surface scattering. The fact that the resistivity arising from different electron scattering mechanism at work in the bulk can be estimated approximately by using Mathiessen's rule using a

TABLE II. Determination of the height-height autocorrelation function, from precision measurements of the topography of the rough surface employing a STM. Parameters t: sample thickness, δ: rms roughness amplitude. ξ: lateral correlation length, corresponding to a Gaussian representation of the autocorrelation function $h(x, y) = \delta^2 \exp[-(x^2 + y^2)/\xi^2]$, considering the roughness parameters measured on different sites: Grain Terraces (GT), Grain Side (GS), and Grain Boundary (GB). The column χ^2/ν represents the goodness of the fit over more than ten thousand data points per sample, e.g., the statistical error χ^2 over the number of data points ν of the fit. Data taken from Table II of Ref. 69 with permission.

Site	t (nm)	δ (nm)	ξ (nm)	χ^2/ν
GT	54	0.049	1.8	1.0
	96	0.055	2.2	0.5
	135	0.057	1.5	0.5
	255	0.098	2.0	0.4
GS	54	0.097	2.7	0.3
	96	0.067	1.4	0.3
	135	0.052	1.4	1.4
	255	0.088	2.0	0.6
GB	54	0.38	3.3	0.7
	96	0.42	3.9	0.5
	135	0.48	3.5	0.6
	255	0.46	2.3	0.7

classical description of size effects (based upon solutions of BTE employing the relaxation time approximation to describe the effects of different electron scattering mechanisms) is in sharp contrast to the resistivity arising from electron-rough surface scattering. This issue has been discussed in Ref. 41. It has also been discussed in the case of the resistivity of $CoSi_2$ films, for it turns out that the observed resistivity at 4 K of a 10 nm thick $CoSi_2$ film is about twice as large as the resistivity of the film estimated by using Mathiessen's rule, as displayed in Fig. 16. As discussed in Ref. 70, the quantum description of charge transport assigns an important role to the identity of the states occupied by the electron. Such an important role is reflected in the fact that, regardless of the different approximations involved, all quantum theories of size effects described in Section II C lead to a resistivity that depends explicitly upon the sub band index n that identifies the quantum states participating in the charge transport process. Furthermore (we quote),

> "The question naturally arises. Why is Mathiessen's rule violated?…"
>
> "…because the quantum description of charge transport assigns an important role to the identity of the states occupied by the electron… This is in contrast to bulk scattering, where the fact that the metallic sample takes the form of a thin film (and the electron momentum perpendicular to the film is quantized as a consequence of the confinement of the electron gas between two parallel potential barriers) is irrelevant, and hence the corresponding resistivity is independent of the identity of the electron states."

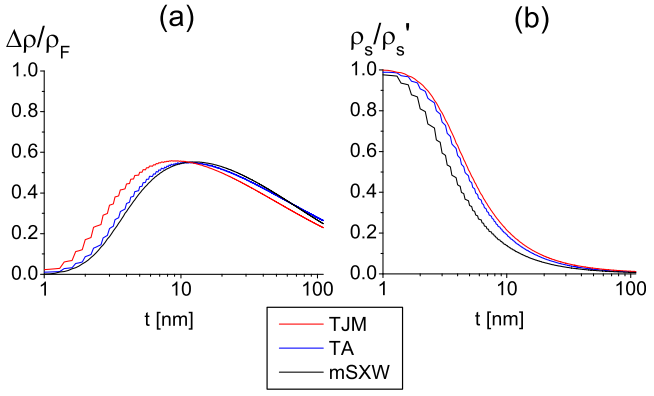

FIG. 16. Violations of Mathiessen's rule in $CoSi_2$ films. (a) $\Delta\rho/\rho_F = [\rho_F - (\rho_S + \rho_B)]/\rho_F$ plotted as a function of film thickness, where ρ_F is the resistivity of the film, ρ_S is the resistivity induced by electron-surface scattering, and ρ_B is the resistivity of the bulk. TJM, theory of Tesanovic, Jaric and Maekawa (Ref. 45), with $\delta = 0.5$ nm. TA, theory of Trivedi and Aschroft (Ref. 47), with $\delta = 0.75$ nm. mSXW, modified theory of Sheng, Xing, and Wang (Ref. 28), using a Gaussian ACF with $\delta = 0.2$ nm, $\xi = 0.5$ nm. (b) Ratio between the surface resistivity ρ_S and *the apparent surface-induced resistivity* $\rho_S' = \rho_F - \rho_B$ predicted by different models by applying Mathiessen's rule, plotted versus film thickness. The apparent surface resistivity ρ_S' turns out to be about an order of magnitude larger than the surface resistivity ρ_S except in films that are only a few nanometers thick. Data taken from Fig. 2 of Ref. 70 with permission.

> "…as a consequence of the fact that the electronic states are quantized and because of the importance of the identity of the electron states within the quantum description of charge transport, the additivity of the scattering rates (stemming from the statistical independence between averaging over impurities or over the phonon population in the case of bulk scattering, and averaging over surface roughness configurations in the case of surface scattering) no longer leads to the additivity of the corresponding resistivities, consequently Mathiessen's rule no longer holds" (Ref. 70, pp. L182–L183).

Then, the proper question to ask is: Under what conditions should Mathiessen's rule be a valid approximation to estimate the increase in resistivity induced by electron-surface scattering? The answer is, we might expect the additivity rule to be recovered, *when counting over quantized states becomes irrelevant,* that is, *for samples that are thick enough to contain hundreds of electron states…* (Ref. 70, p. L183). According to Fig. 16(a), the observed resistivity of a 10 nm thick $CoSi_2$ film *is about twice as large as what can be estimated by using Mathiessen's rule*.

A similar situation holds regarding the quantum theory of electron-grain boundary scattering, in that the observed resistivity of the thin film is expected to *severely violate* the additivity rule regarding the resistivity of the bulk (in the absence of grain boundaries) plus the resistivity arising from electron-grain boundary scattering acting in the absence of electron scattering in the bulk, that is, in a sample where the bulk resistivity is very small, where the bulk mean free path is very long. In the limit of a very long mean free path $\ell(T)$, the resistivity arising from electron-grain boundary scattering diverges exponentially with $\ell(T)$, because of weak Anderson localization induced by electron scattering on disordered grain boundaries, as will be discussed later.

We now abandon any attempt to describe theoretically the magnetomorphic coefficients and focus only on the ability of quantum transport theories to describe the temperature and thickness dependence of the resistivity observed in thin gold films made out of columnar grains in the absence of magnetic field (in samples where the Hall mobility μ_H is proportional to the film thickness t at 4 K), at temperatures T, $4\,K < T < 300\,K$, using as input data the parameters (δ, ξ) that describe the average surface roughness measured with a STM on each sample. The discussion focuses on those quantum theories where electron-grain boundary scattering can be neglected, and the resistivity can be computed directly in terms of (δ, ξ): the theory of Tesanovic, Jaric, and Maekawa,[45,46] the theory of Trivedi and Aschroft,[47] the mSXW theory,[28] and the mSXW fractal theory.[50]

Employing the values (δ, ξ) measured on each sample with the STM as input data, using the method of resistivity data analysis described in Section II C, we determined the average distance traveled by an electron between collisions $\ell_0(T) = v_F\tau_0(T)$, representing *the mean free path in the bulk, in a sample having the same concentration of impurities/point defects as the thin film, but where electron-surface scattering has been switched off*. The values of the residual

resistivity $\rho_0(4)$ emerging from data analysis involving different theoretical models are listed in Table III. The results of data analysis seem interesting: *The quantum theories of size effects do exhibit a predicting power,* in the sense that we can roughly estimate (to within 10% or better, regardless of the film thickness) what the resistivity of a thin metallic film would be at different temperatures, from the typical parameters that characterize the average surface roughness, which could be measured routinely with an AFM/STM endowed with atomic resolution.

3. The bulk resistivity

Nevertheless, there is a remarkable result: The bulk resistivity $\rho_0(4)$ predicted by *any of the theoretical models* depends on the model employed to analyze resistivity data, *but it decreases at least by a factor of 4 between the 54 nm thick film and the 255 nm film regardless of the theoretical model*. We quote:

> "…the residual bulk resistivity corresponding to each sample turns out to depend on film thickness, *a result that is at variance with the central assumption used for decades to analyze thin film resistivity data*. This can be considered a severe warning regarding the applicability of resistivity data analysis based upon parameter fitting performed over many decades. Not only because electron-grain boundary scattering may have contributed a significant amount to the observed resistivity data reported by many other authors, but because such data analysis is based upon a simplifying assumption *whose validity seems questionable: The assumption that the parameters characterizing the bulk, for a family of films of the same metal prepared under similar conditions of evaporation, are independent of film thickness*. A bulk resistivity that varies with film thickness may be understood as arising from a concentration of impurities/defects present in the samples that varies with film thickness. The residual resistivity observed in crystalline samples is known to depend on the impurity/defect concentration" (Ref. 69, p. 3403).

TABLE III. Residual resistivity $\rho(4)$. Experimental residual resistivity $\rho(4)$ corresponding to Drude's model, and theoretical residual resistivity $\rho_0(4)$ of the bulk, according to different models, considering the roughness parameters measured on different sites (GT: Grain Terrace, GS: Grain Side, GB: Grain Boundary). The different theoretical models are TA: Trivedi and Aschroft (Ref. 47). TJM: Tesanovic, Jaric and Maekawa (Refs. 45 and 46). Calecki (Ref. 26). FS: Fuchs-Sondheimer (Ref. 11). mSXW: Modified theory of Sheng, Xing and Wang (Ref. 28). Data taken from Table 3 of Ref. 69 with permission.

				$\rho_0(4)$			
Site	t (nm)	Drude (nΩ m)	TA (nΩ m)	TJM (nΩ m)	Calecki (nΩ m)	FS (nΩ m)	mSXW (nΩ m)
GT	54	7.6	7.5	7.5	7.5	4.0	6.0
	96	4.1	4.1	4.0	4.1	2.1	3.1
	135	2.6	2.6	2.5	2.6	1.2	1.9
	255	1.7	1.6	1.6	1.7	0.9	1.0
GS	54	7.6	7.4	7.2	7.5	4.0	4.5
	96	4.1	4.0	4.0	4.1	2.1	2.9
	135	2.6	2.6	2.5	2.6	1.2	2.0
	255	1.7	1.6	1.6	1.7	0.9	1.1
GB	54	7.6	5.2	4.1	7.5	4.0	3.9
	96	4.1	2.6	2.0	4.1	2.1	2.2
	135	2.6	1.4	1.0	2.6	1.2	1.4
	255	1.7	1.0	0.8	1.7	0.9	1.0

One aspect that is unexpected is that *the accuracy of the temperature dependence of the resistivity predicted by Drude's model published in 1900 seems comparable to the predictions based upon models published several decades later,* such as Fuchs-Sondheimer (FS), Tesanovic-Jaric-Maekawa (TJM), Trivedi-Aschroft (TA), Calecki, and the modified theory of Sheng, Xing, and Wang (mSXW). The fact that the predictions based upon Drude's model turns out to be comparable to the predictions based upon other quantum models, and that this holds even for the thinnest (54 nm thick) film, implies that the increase in resistivity arising from electron rough-surface scattering at 300 K is of the order of a few percent in these gold films.[69]

Regarding the modified mSXW theory describing electron scattering by a rough fractal surface, we found that when $d < 0.5\ \ell_0(300)$, then *the dominant electron scattering mechanism controlling the resistivity is not electron-surface scattering but rather electron-grain boundary scattering, and the later electron scattering mechanism is not included in the theory* (Ref. 51, p. 023710-8).

Another point that seems relevant is that *the small increase in resistivity at 4 K* (*of the order of a few % or less*) induced by electron-surface scattering predicted by the Calecki, TJM, or TA models, when using the measured surface roughness, *is in contradiction with the temperature dependence of the magnetomorphic coefficients measured at low temperatures:* the temperature dependence of the Hall mobility $\mu_H(T)$ (Ref. 65 and Fig. 10), of the transverse magnetoresistance and of the longitudinal magnetoresistance $(\Delta\rho/\rho)(T)$ (Figs. 11–13). For at 4 K, $\mu_H(4)$ depends linearly on film thickness, and the transverse as well as the longitudinal $(\Delta\rho/\rho)(4)$ measured at 9 T increases with increasing film thickness t, signaling the predominance of electron-surface scattering at 4 K. Increasing T to 50 K results in a decrease of $\mu_H(50)$ by over a factor of two,[64,65] while the transverse and the longitudinal $(\Delta\rho/\rho)(50)$ decreases by about a factor of four,[60–63] indicating that at 50 K *electron-phonon scattering becomes dominant*. The fact that, based upon the measurement of these magnetomorphic effects, *electron-surface scattering dominates charge transport and the resistivity observed at 4 K but at 50 K electron-phonon scattering is the dominant scattering mechanism* contradicts the small variation of the ratio $\rho(T)/\rho_0(T)$ with respect to unity between 4 K and 300 K, predicted by Calecki, TA, and TJM. The theories that do predict a variation of $\rho(T)/\rho_0(T)$ that would seem consistent with the measurement of these magnetomorphic effects, indicating the predominance of electron-surface scattering at 4 K but electron-phonon scattering at $T > 50$ K, are the classical Sondheimer model and its quantum version, the mSXW theory.

Finally, there is one other aspect regarding the ratio ρ/ρ_0 predicted by different quantum transport theories regarding a

markedly different dependence on the scale of length involved in electron-surface scattering. A quantum description of electron-rough surface scattering is expected to exhibit the ability *to select the corrugations that effectively contribute to scatter off the electrons*. Based upon arguments borrowed from geometrical optics, we intuitively expect that the corrugations that contribute effectively are those that take place, say, within a scale of distance comparable to the Fermi wave length λ_F (to within an order of magnitude).[69,71] While the models TA, TJM, and Calecki predict a monotonic increase in the ratio ρ/ρ_0 with increasing δ, the mSXW turns out to be the only quantum model that predicts an increase in resistivity that takes on its maximum value at around $\delta/\lambda_F \approx 0.4$ (for $\xi = 2.0$ nm) and then asymptotically approaches unity with further increasing δ beyond this maximum, as displayed in Figure 17. This confirms our preliminary finding.[71]

V. RESISTIVITY DATA AND PREDICTIONS OF THEORIES OF ELECTRON-GRAIN BOUNDARY SCATTERING

To assess the predictive power of the MS theory and of the quantum theory, it becomes necessary to prepare thin films where the film thickness and the grain diameter making up the samples are independent variables; we succeeded in preparing gold films evaporated onto mica substrates where t and d are varied independently;[51,65,72] we prepared families of gold films with a thickness of approximately 50 nm and 100 nm, made out of grains where the average grain diameter d describing the Gaussian population of grains varies in the range $11\,\text{nm} < d < 159\,\text{nm}$. This is the relevant range, for the intrinsic electronic mean free path arising from electron-phonon scattering in crystalline Au at 300 K is $\ell_{Au}(300) = 39$ nm.

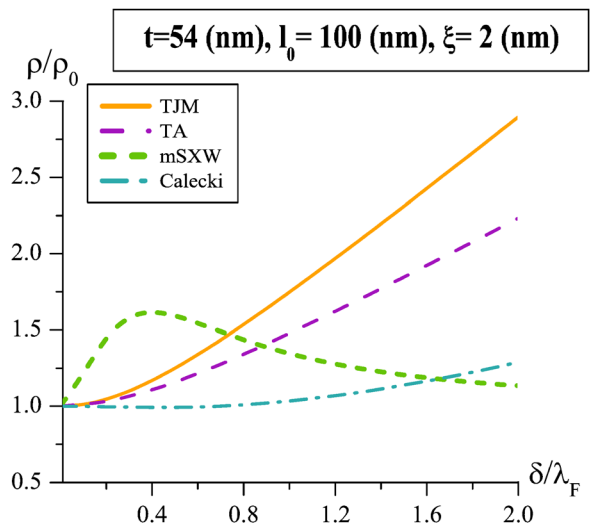

FIG. 17. Comparison between the predictions of different quantum transport theories in the 54 nm thick film, regarding the dependence of the increase in resistivity ρ/ρ_0 on the scale of distances involved in electron-surface scattering, determined by δ, the rms roughness amplitude of the Gaussian autocorrelation function, measured in units of the Fermi wave length for Au ($\lambda_F = 0.52$ nm). Typical (representative) values of $\xi = 2.00$ nm, and $\ell_0 = 100$ nm, were used. TJM: theory of Tesanovic, Jaric, and Maekawa. TA: theory of Trivedi and Aschroft. mSXW: modified theory of Sheng, Xing and Wang. Data taken from Fig. 9 of Ref. 69 with permission.

It seems interesting to test the predictions of the theories describing electron-grain boundary scattering in two special cases: (A) Thin films made out of columnar grains extending from top to bottom, where the measurement of the Hall effect indicates that the resistivity of the film at 4 K is controlled by electron-rough surface scattering; in this case, the Hall mobility μ_H turns out to depend linearly on film thickness t (Fig. 9). (B) Thin films made out of grains whose diameter d is smaller than $\ell_0(300)$, where measuring the Hall effect indicates that the resistivity of the film at 4 K is controlled by electron-grain boundary scattering, for in this case the Hall mobility μ_H turns out to depend linearly on the grain diameter d (Fig. 9) *regardless of film thickness*.

To properly perform such a comparison between theory and experiment, the resistivity of each specimen was measured as a function of temperature T; $4\,\text{K} < T < 300\,\text{K}$, and the surface roughness as well as the distribution of grain sizes of each sample were measured in independent experiments. Attention should be paid to case (B), for we are not aware of any study that has been published, where the temperature dependence of the resistivity of samples satisfying $d < [\ell_{Au}(300) = 39\,\text{nm}, t]$ has been measured at temperatures T, $4\,\text{K} < T < 300\,\text{K}$, and where the surface roughness as well as grain size distribution have been measured on each sample. Case (B) is interesting for we expect that the metallic interconnects in IC's will be made by depositing the metal in trenches that have been prepared in the semiconductor wafer, where the width of the trenches is expected to fall below 10 nm within the next decade. Hence, we may expect that the grain diameter of the metal making up such interconnects may be of the order of or smaller than 10 nm, and consequently, we expect that electron-grain boundary scattering may be the dominant electron scattering mechanism controlling the resistivity of such interconnects at room temperature.

We published the results of these experiments in Ref. 72. The temperature dependence of the resistivity of different samples as well as the ratio between the resistivity $\rho(T)$ measured on each sample and the resistivity $\rho_0(T)$ of the bulk (according to MS theory) are displayed in Fig. 18. There are two results that seem remarkable. First, using data analysis based upon parameter fitting, a set of parameters can be found within the MS theory, which describes with fair accuracy the temperature and thickness dependence of the resistivity data, even for films made out of small grains. Second, in spite of such fair agreement between theory and experiment, it seems odd that the grain boundary reflectivity R needed to explain the data for the films where $d \leq 13$ nm, is $0.3 \leq R \leq 0.43$ [Table 1 in Ref. 72], and that the ratio $\rho(4)/\rho_0(4)$ for these films is larger than 100!!

As a consequence of this parameter fitting, we stumbled on the fact that one of the assumptions on which the MS model stands, a first order perturbation theory, is at variance with this resistivity data analysis: *the effect of rough surfaces and grain boundaries in small grained films leads to an increase in resistivity which is about two orders of magnitude at 4 K, and the grain boundary reflectivity needed to describe the temperature dependence of the data in small grained films is R > 30%, which means that over 30% of the electrons are reflected upon colliding with the very first grain boundary.*

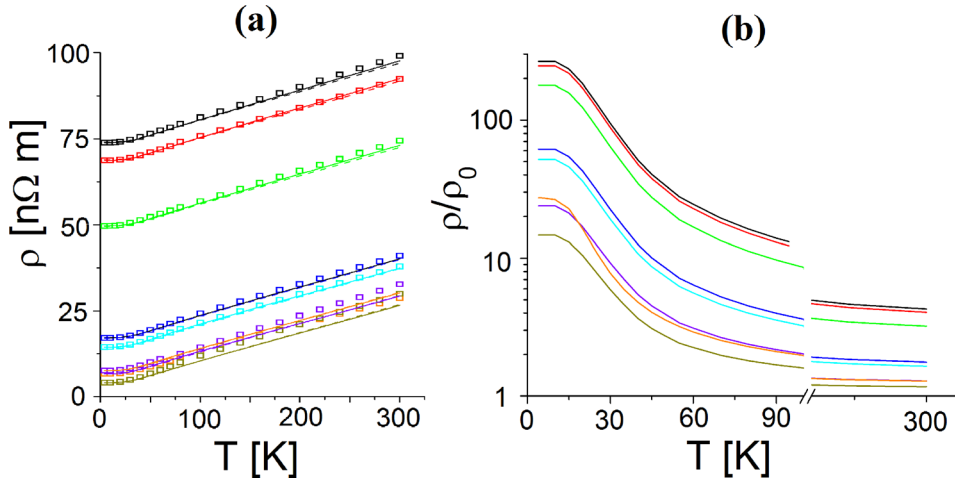

FIG. 18. (a) Comparison between the temperature dependence of the resistivity data on thin gold films deposited onto mica substrates, with the theoretical predictions based upon the theory of Mayadas and Shatzkes (MS) and the theory of Palasantzas (P). Empty symbols: resistivity data. Black Squares, S1 (t = 49 nm, d = 11.1 nm). Red Squares, S2 (t = 109 nm, d = 12.4 nm). Green squares, S3 (t = 42 nm, d = 13.0 nm). Blue squares, S4 (t = 96 nm, d = 15.8 nm). Light-blue squares, S5 (t = 50.0 nm, d = 24.1 nm). Orange squares, S6 (t = 97 nm, d = 37.5 nm). Violet squares, S7 (t = 54 nm, d = 106 nm). Brown squares, S8 (t = 96 nm, d = 159 nm). Solid line: Predictions based upon MS theory for $p_0 = p_t = 0$ in samples S1 through S6, and $p_t = 0$ $p_0 = 1$ for samples S7 and S8. Dashed line: Predictions based upon the theory of Palasantzas (Ref. 113). (b) Temperature dependence of the increase in resistivity $\rho(T)/\rho_0(T)$ predicted by the theory of Mayadas and Shatzkes, arising from electron-surface and electron-grain boundary scattering. Data taken from Figs. 2 and 3 of Ref. 72 with permission.

Can these MS predictions be trusted? Are the fitting parameters [R, $\ell_0(4) = \ell_{IMP}$] displayed in Table I leading to these predictions, unique? In the final analysis, does the MS theory really have a predicting power, or could the agreement between MS theoretical predictions and experimental resistivity data obtained via parameter fitting, be considered a consequence of some numerical accident? Why?

This confusing situation led us to revise our own work and to suspect that the agreement between the resistivity predicted by MS theory and the observed resistivity was some sort of accident, that the fitting parameters used to produce resistivity curves (that exhibited such a nice and fair agreement with the data, as displayed in Fig. 18) were, perhaps, not unique, and that maybe the classical theory does not really have a predictive power for small grained samples, and that the parameters estimated via the fitting process were, perhaps, not very meaningful, as has been assumed by so many researchers for decades.

In order to assess the predictive power of the Classical MS theory and of the quantum theory, we have chosen to analyse data from samples S1, S2, S7, and S8 from Ref. 72. From arguments contained in Section III, we know that in samples S1 and S2, electron-grain boundary scattering is dominant at 4 K, for the Hall mobility μ_H turns out to be proportional to the grain diameter d *regardless of the film thickness*. On the contrary, samples S7 and S8 are made out of columnar grains extending from top to bottom; from arguments contained in Section III, we know that in samples S7 and S8, electron-rough surface scattering is dominant at 4 K, for the Hall mobility μ_H turns out to be *proportional to the film thickness t*.

We start by stressing the fact that the predictions of MS theory depend on the individual properties of the grain boundaries (for example, on its reflectivity R). This is in contrast to the quantum theory, where the increase in resistivity of the thin film over the bulk is controlled by the *collective properties of the assembly of grain boundaries*.

The first *collective property of the assembly of grain boundaries* that produces a decrease in the conductivity of the film is the forbidden KP bands projected onto the Fermi sphere, as illustrated in Figs. 3 and 4.

The second *collective property* that increases the resistivity of the thin film is electron scattering by an assembly of N disordered grain boundaries found along a bulk mean free path, that (because of the exponential decay of the electron wave function with distance induced by electron scattering from a disordered 1-D potential) leads to a transmission coefficient $T_N < 1$, which reduces the conductivity. This is illustrated in Fig. 19 where we compare the ratio σ/σ_0

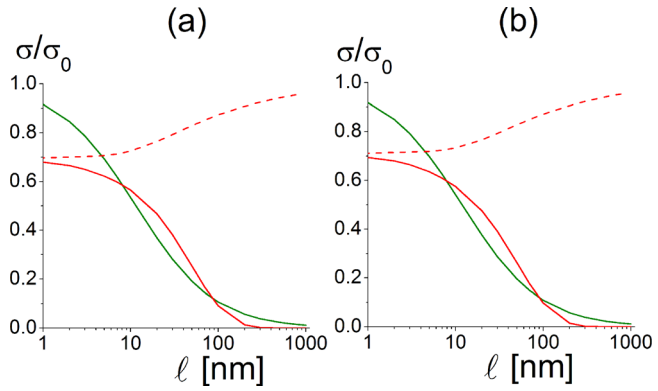

FIG. 19. Dependence of the ratio σ/σ_0 on the bulk mean free path ℓ. σ is the conductivity of a crystalline metal including an array of grain boundaries represented by Eq. (30), σ_0 represents the conductivity of the bulk (in the absence of grains). Green solid line: Predictions of MS theory with $p_0 = p_t = 1$. Red dashed line: predictions of the quantum theory [Eq. (36) with $T_N = 1$]. Red solid line: predictions of the quantum theory [Eq. (36) with $T_N < 1$] employing parameters listed in Table I. (a) Predictions for sample S1. (b) Predictions for sample S2. Data taken from Fig. 2 of Ref. 7 with permission.

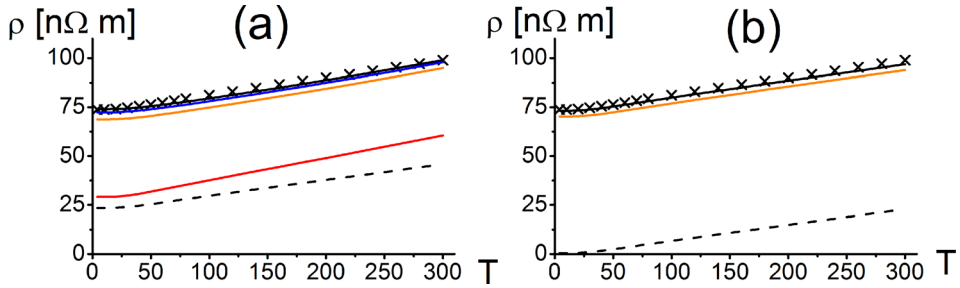

FIG. 20. (a) Temperature dependence of the resistivity predicted by the quantum theory [Eq. (41)] for sample S1, employing the parameters listed on Table I. Crosses: experimental data, sample S1. Dashed black line: ρ_0 (resistivity of the bulk), arising from electron-phonon + electron-impurity scattering. Red solid line: $\rho_0 + KP$ (Kronig-Penney) potential representing uniformly distributed grain boundaries computed from Eq. (36) with $T_N = 1$. Orange solid line: $\rho_0 + KP + D$ (Disorder) computed from Eq. (36) with $T_N < 1$. Blue solid line: Resistivity of the thin film (TF) $\rho_0 + KP + D + TF$, computed from Eq. (41) with $T_N < 1$. Black solid line: Resistivity of the thin film + rough surface (RS) $\rho_0 + KP + D + TF + RS$, the effect of the rough surface is computed by shifting the Fermi sphere, as explained in Section II E (b) Temperature dependence of the resistivity predicted by the classical theory [Eq. (27)] for sample S1, employing the parameters listed on Table I. Crosses: experimental data, sample S1. Dashed black line: ρ_0 (resistivity of the bulk). Orange solid line: $\rho_0 + MS$, computed from Eq. (27) with R listed in Table I, $p_0 = p_t = 1$. Black solid line: Resistivity of the thin film + rough surface (RS) $\rho_0 + MS + RS$, computed from Eq. (27) with R listed in Table I, $p_0 = 0$, $p_t = 1$. Data taken from Fig. 3 of Ref. 7 with permission.

predicted by the classical and by the quantum theory for samples S1 and S2, where σ represents the conductivity of the crystalline sample containing grain boundaries, and σ_0 is the bulk conductivity. It seems remarkable that the classical prediction approaches zero as ℓ grows larger towards 1 μm, while the quantum prediction (with $T_N = 1$) approaches unity from below. Contrary to the classical MS theory, the decrease in conductivity with increasing ℓ within the quantum theory occurs not because electrons are partially reflected at *one* grain boundary, but because the carriers are transmitted with a probability $T_N < 1$ across successive (disordered) grains.

A. Predictive power of the theory of Mayadas and Shatzkes, and of the quantum theory of electron-grain boundary scattering

To compare the predictions of both the classical and the quantum theory with resistivity data, it becomes necessary to estimate the unknown parameters. The quantum theory contains the unknown parameters ℓ_{IMP} (the unknown electron mean free path at 4 K attributable to electron scattering from randomly distributed impurity/point defects present on each sample) and R (the grain boundary reflectivity); the classical theory contains the additional (unknown) parameters p_0 and p_t (the reflectivity of the two surfaces limiting the film). We set $p_0 = 1$ and $p_t = 0$ in MS theory (because the AFM reveals that mica has atomically flat regions whose linear dimensions extend over several hundred nm); with these assumptions, both the classical as well as the quantum theory now involve only two parameters, R and ℓ_{IMP}. We analyze below the temperature and thickness dependence of the resistivity of samples S1 and S2 using the standard temperature dependent resistivity data arising from electron-phonon scattering available for crystalline gold,[10] employing the method described in Section II to estimate R and to determine the temperature-dependent bulk mean free path $\ell_0(T)$ and $\rho_0(T)$ at $T > 4$ K. The appropriate parameters used in the analysis are listed in Table I; the results of the resistivity data analysis are displayed in Figs. 20 and 21 for small grained samples S1 and S2.

It seems remarkable that both the MS and the quantum theory provide a fair description of the resistivity data and yet, *the phenomena involved underlying the resistivity increase according to the MS theory and according to the quantum model are markedly different*.

For large (columnar) grained samples where $d > \ell(300)$ [$\ell(300) = 39$ nm for Au], the classical theory requires a reflectivity of about $R = 0.22$–0.28 to explain the data, quite large for a first order perturbation theory!! This is in contrast to the quantum description, where the increase in resistivity over the bulk (when turning on the KP potential) is relatively modest, and is attributed not to partial reflection of the electrons from grain boundaries, but to *a decrease in the number of states at the Fermi sphere that are allowed bands of the KP potential; consequently, the reflectivity R required turns out to be an order of magnitude smaller*. For large grained samples, the Anderson localization length L_{LOC} is large enough such that it has a negligible effect on the resistivity.

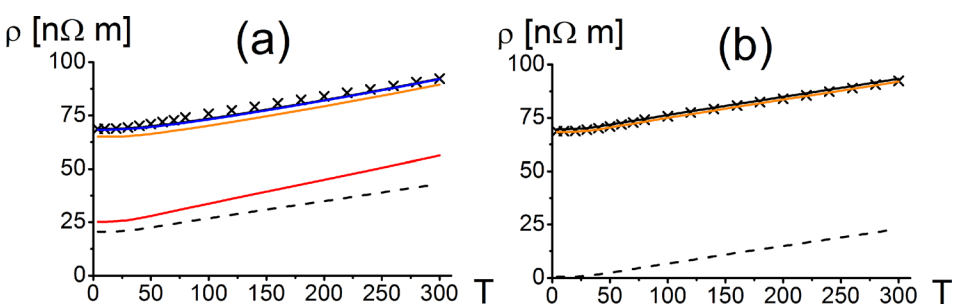

FIG. 21. (a) Temperature dependence of the resistivity predicted by the quantum theory [Eq. (41)] for sample S2, employing the parameters listed on Table I. Symbols as in Fig. 20. (b) Temperature dependence of the resistivity predicted by the classical theory [Eq. (27)] for sample S2, employing the parameters listed on Table I. Symbols as in Fig. 20. Data taken from Fig. 3 of Ref. 7 with permission.

In the opposite case of small grained samples such that $d < \ell(300)$, a huge $R > 0.4$ is required by MS theory (meaning that *over 40% of the electrons are reflected upon colliding with the very first grain boundary, calculated using first order perturbation theory!!*). This is in contrast to the quantum theory, where the increase in resistivity arising from turning on the KP potential is relatively modest; most of the increase in resistivity over the bulk arises not from partial reflection of the electrons from grain boundaries, *but is due instead to weak Anderson localization induced by electron scattering from successive disordered grain boundaries characterized by a localization length of the order of 110 nm*. The reflectivity required by the quantum theory turns out to be about 25% of that required by the classical MS model. In this case, the small localization length definitely affects the resistivity of small grained samples; the dominant mechanism responsible for the increase in resistivity is the exponential decay of the electron wave function with increasing distance induced by electron scattering from (small) disordered grains.

However, we have not answered yet one of the fundamental questions that motivated this study: How reliable are the predictions based upon these two theories? Are the parameters selected to describe the resistivity data significant, reliable, and unique? What is the predictive power of the classical theory and of the quantum theory?

To compare quantitatively the description of the resistivity data furnished by both theories, we use as a statistical parameter measuring the goodness of the theoretical description, the Standard Statistical Error (SSE) $\mathrm{SSE} = \sqrt{\frac{1}{N-2}\sum_{i=1}^{N}\left[\frac{\left(\rho_{exp}(T_i)-\rho_{theo}(T_i)\right)^2}{\rho_{exp}(T_i)^2}\right]}$, where $\rho_{exp}(T_i)$ and $\rho_{theo}(T_i)$ stand for the resistivity measured (exp) and theoretically predicted (theo), respectively, at each of the $N = 20$ different temperatures $4\,K \le T_i \le 300\,K$ at which the resistivity was measured on these samples (resistivity data taken from Ref. 72). This constitutes a stringent test, for changing temperature from 4 K to 300 K changes the bulk mean free path ℓ_0 continuously on each sample, so for each specimen, we have 20 resistivity data points where the ratio ℓ_0/t and ℓ_0/d varies substantially. We used SSE to assess the goodness of the theoretical description, varying the parameters R and ℓ_{IMP} in the neighborhood of the parameters listed in Table I. The result of this comparative error analysis is displayed in Figures 22 and 23 for samples S1 and S2. Similar results (not shown) were obtained for samples S7 and S8.

The results displayed in these figures came as a surprise to us. It seems remarkable that in order to generate the 2-D plot [displaying the different levels of the statistical error SSE induced by changing the parameters (ℓ_{IMP}, R) using the classical MS theory, *we were forced to use a logarithmic scale, as opposed to the linear scale used in the case of the quantum theory*. For it turns out that the resistivity data predicted by the Mayadas and Shatzkes theory—that has been widely used for decades by many researchers in the field—*can be described using many sets of (ℓ_{IMP}, R); consequently, the fitting parameters are unreliable, their significance as well as the predictive power of MS theory seems highly questionable*. This is in contrast to the predictive power of the quantum theory, where for each sample, a unique set of (ℓ_{IMP}, R) can be found—say, to within ±10% or better—to describe the resistivity data.

The quantum theory presented here exhibits yet another new and interesting feature, a strong interference between electron scattering in the bulk (B), and electron scattering by grain boundaries (GB) in a crystalline sample containing grains. In the limit of a very pure crystalline sample cooled to 4 K carrying a very small concentration of point defects, where the phonons are frozen out ($\lim \ell \to \infty$), the resistivity arising from electron-grain boundary scattering alone ρ_{GB} *diverges* as an increasing exponential of ℓ with increasing bulk mean free path on account of Anderson localization. Hence, we expect that the observed resistivity of the specimen ρ_S is such that $\rho_S \neq \rho_B + \rho_{GB}$, where ρ_B is the resistivity of the bulk. Consequently, we expect Mathiessen's rule to be severely violated in nanometric specimens made out of pure metal having small disordered grains, where quantum effects should dominate charge transport.

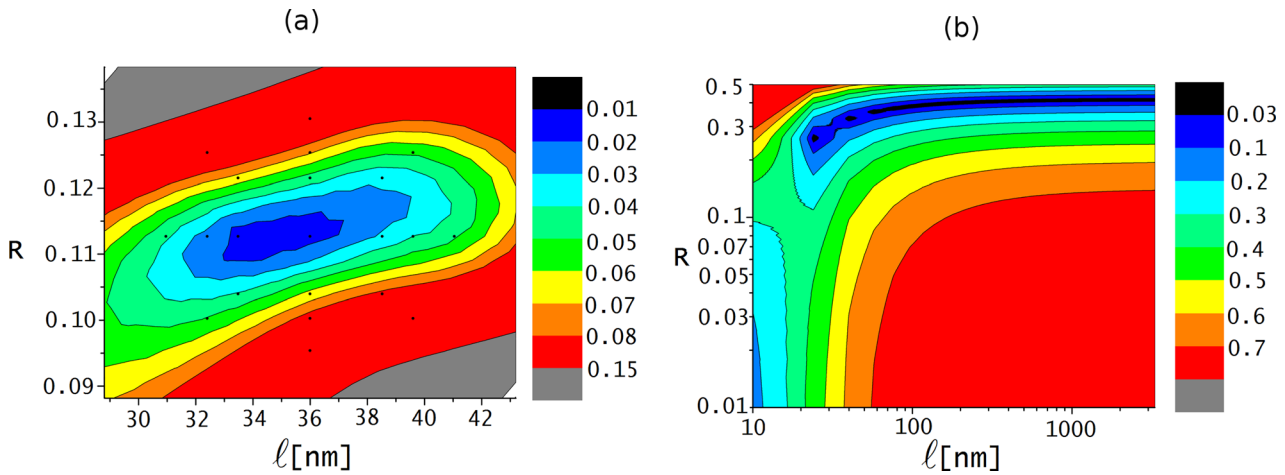

FIG. 22. (a) Predictive power of the quantum theory, varying the parameters (ℓ_{IMP}, R) in the neighborhood of the parameters listed in Table I, needed to furnish a fair description of the temperature dependence of the resistivity data on sample S1. The plot displays different levels the Standard Statistical Error, SSE (indicated by different colors), as a function of the parameters (ℓ_{IMP}, R). (b) Predictive power of the classical theory for sample S1.

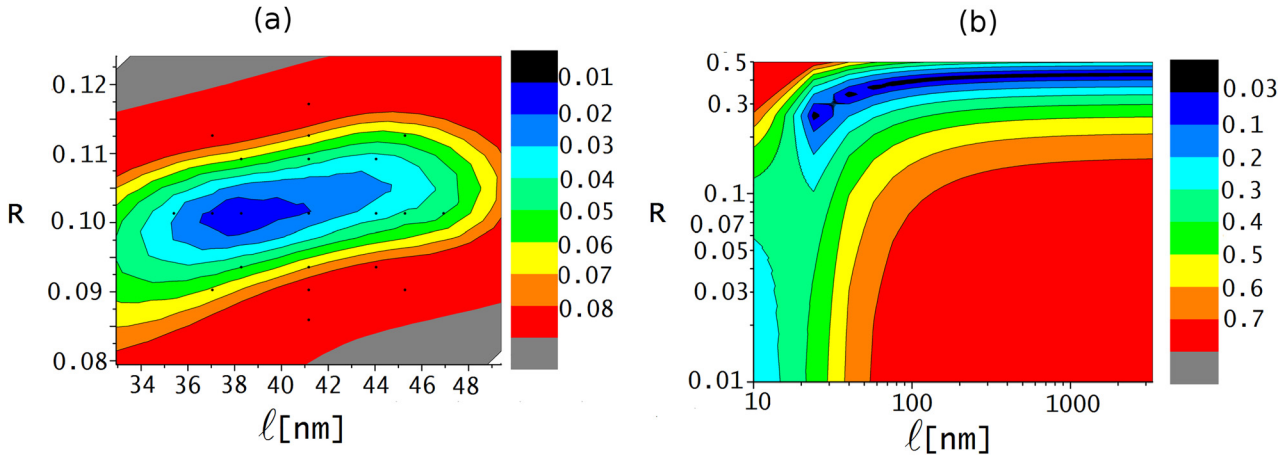

FIG. 23. (a) Predictive power of the quantum theory, varying the parameters (ℓ_{IMP}, R) in the neighborhood of the parameters listed on Table I, needed to furnish a fair description of the temperature dependence of the resistivity data on sample S2. The plot displays different levels the Standard Statistical Error SSE indicated by different colors, as a function of the parameters (ℓ_{IMP}, R). (b) Predictive power of the classical theory for sample S2.

VI. ESTIMATION OF THE RESISTIVITY OF NANOMETRIC Cu WIRES OF RECTANGULAR CROSS SECTION

An interesting application of the formalism discussed in Section II is an evaluation of the ability of the new quantum theory of electron-grain boundary scattering to describe the resistivity of nanometric Cu wires of rectangular cross section. In order to explore such an ability, we computed the resistivity of nanometric Cu wires of rectangular cross section employed in IC design, using Equation (42), in an attempt to explain the resistivity measured at room temperature reported in Ref. 73. To perform this calculation, we used the analytical representation of the transmission coefficient T_N discussed in Section II, employing the Fermi wave vector k_F appropriate for Cu. As a first approximation, we neglected the contribution to the resistivity arising from electron-rough surface scattering, as this would have required shifting the Fermi sphere along y (a direction contained in the plane of the Cu lines but perpendicular to the line width) and along z (a direction perpendicular to the plane of the Cu lines), employing the analytical method discussed in Section II. The result of this exploration (neglecting electron-surface scattering) is displayed in Fig. 24.

The results displayed in Fig. 24 indicate that, for each wire of rectangular cross section, an impurity mean free path ℓ_{IMP} at 4 K and a grain boundary reflectivity R can be found to describe the resistivity of the wire employing the new theory. Hence, the new quantum theory does exhibit the power of predicting the resistivity of wires of (approximately) rectangular cross section; the values of the parameters displayed in this figure seem coherent with what we found when describing the temperature dependent resistivity of thin gold films discussed in Section V.

However, the description of the resistivity is not unique, for different pairs of (ℓ_{IMP}, R) can be employed to describe the resistivity of the same wire. Based upon the experiments in gold films discussed in Sec. V, experimental information is needed to remove this ambiguity in order to identify the parameters controlling the resistivity of the wire whose width has shrunk (becoming smaller than the electronic mean free path at room temperature): (a) First, the grain size

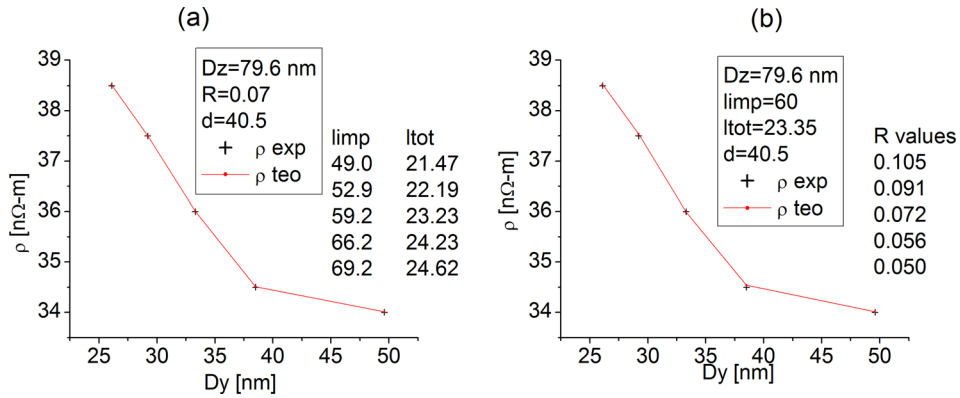

FIG. 24. Comparison between the resistivity of Cu interconnects of rectangular cross section measured at room temperature, and the resistivity predicted by the quantum theory. The trench dimension D_y varies approximately from 26 to 50 nm. The average grain size measured along the trench is 40.5 nm; the height of the trench is 79.6 nm. (a) Resistivity predicted by Eq. (42) neglecting electron-surface scattering, with a fixed grain boundary reflectivity R = 0.07, varying the impurity mean free path ℓ_{IMP}; increasing values of ℓ_{IMP} correspond to increasing values of D_y. (b) Resistivity predicted by Eq. (42) neglecting electron-surface scattering, with a fixed impurity mean free path $\ell_{IMP} = 60$ nm (describing electron scattering in the bulk at 4 K), varying the grain boundary reflectivity R; decreasing values of R correspond to increasing values of D_y.

distribution should be measured along the length of each wire, for disorder on these grains is likely to control the resistivity of the interconnect; (b) second, measuring the resistivity as a function of temperature over a wide temperature range from 300 K down to 4 K (to achieve phonon freeze out and to eliminate the effect of electron-phonon scattering) seems essential.

VII. DISCUSSION

The quantum theory describing electron-surface scattering and electron-grain boundary scattering presented above may contribute to a more realistic estimation of the resistivity of the interconnects used in designing and building IC's, for it is entirely based upon a quantum description of electron motion appropriate for the small scales of distance involved. However, there are a number of issues that remain open, which we briefly address below.

We start by pointing out that the quantum theory of electron-grain boundary scattering presented in Section II E relies upon a coherent quantum description of electron motion which is valid at short scales of distances (distances smaller than the electronic mean free path in the bulk at 300 K); it is primarily intended for wide band simple metals such as Cu, Au, and Al used by the electronic industry today. However, the formalism assumes that the electronic energy levels of the sample are well described by the Fermi energy that characterizes de bulk. We expect that for samples made out of very small grains or very thin films (grain size or film thickness comparable to or smaller than about 2 nm), confinement effects may modify substantially the electronic energy levels within the metal specimen, thereby rendering questionable the predictions of the theory.

A. Electron-surface scattering or electron-grain boundary scattering?

The experiments discussed in Section III B indicate that the dominance of electron-surface scattering or electron-grain boundary scattering is simply determined by the smallest of the scales of length describing each of these electron scattering mechanisms: (1) the sample thickness t, (2) the typical grain diameter D, and (3) the electron mean free path in the bulk $\ell(T)$ at temperature T. To be the dominant electron scattering mechanism, the scale of distance associated with electron-surface scattering (or to electron-grain boundary scattering) needs to be an order of magnitude smaller than the other two scales of lengths involved.

For samples made out of columnar grains (extending from top to bottom), if $t < \ell(T)$ and $t < D$, then electron-surface scattering will be dominant; in this case, the Hall voltage and Hall mobility turns out to be proportional to t, and hence, the average electronic collision time τ depends linearly on t, *which can be considered the finger print of electron-surface scattering being the dominant electron scattering mechanism*. For samples such that $D < \ell(T)$ and $D < t$, then electron-grain boundary scattering will be the dominant electron scattering mechanism, for in this case the average electronic collision time τ turns out to be proportional to D *regardless* of film thickness t; *this can be considered the finger print of electron-grain boundary scattering being dominant electron scattering mechanism*. When D is comparable to t and/or D is comparable to $\ell(T)$, then the resistivity involves a combination of all the electron scattering mechanisms whose characteristic scale of lengths are comparable.

One of the outstanding issues is whether electron-surface or electron grain boundary scattering becomes the dominant electron scattering mechanism regarding the increase in resistivity induced by size effects in nanometric interconnects with shrinking dimensions. There are reports that electron-surface scattering is dominant in Cu wires.[74–76] However, other researchers have found that electron-grain boundary scattering is dominant in thin Cu films[77–82] and Cu wires.[83] Although at first glance these conclusions might seem to contradict each other, they may be related to the fact that we expect electron-surface scattering to play a more important role in thin wires than in thin films, for the surface to volume ratio is larger in the former.

The relevant question is related to the role played by the resistivity induced by electron-grain boundary scattering as compared to the resistivity arising from electron-surface scattering, and when should the former become the dominant scattering mechanism responsible for the increase in resistivity of interconnects. From the experiments described in Section III, we expect this will occur when D becomes smaller than the electron mean free path $\ell(T)$ in the bulk (associated with the interconnect) at temperature T, and becomes comparable to or smaller than the width of the interconnect. Moreover, there is the experimental certainty that, (contrary to the conceptual picture underlying MS theory—where the resistivity originates from electron scattering at a single grain boundary), large discrete resistance jumps have been reported at grain boundaries present in Au films[84] and in Cu nanowires,[85] the observation employed a STM equipped with a 4 probe measuring device, an instrument called Scanning Tunnelling Potentiometer.

As long as the interconnects are made out of a metal deposited onto deep and narrow trenches on a Si wafer, it would appear that the grain diameter D will be limited by the width of the trenches. Decreasing the dimensions of the latter may probably lead to electron-grain boundary scattering playing the role of dominant electron scattering mechanism controlling the resistivity.

Within this context it seems relevant to quote the conclusions mentioned in a recent review:

> "…Measuring cross-sectional dimensions is conceptually straightforward, but when the height and width of cross sections are only several tens of nanometers, such measurements can be extremely challenging in practice. The accuracy of the numbers extracted from images (obtained with focused ion beams) can also be operator dependent. Furthermore, dimensions can vary significantly along the length of the line" (Ref. 86, p. 246).

The natural question that arises then is, how can the quantum formalism contained in Section II E be used to estimate the increase in resistivity arising from electron-surface scattering? The answer is, the quantum formalism is based

upon the assumption that two of the surfaces limiting the electron gas are approximately parallel (to within a few percent of each other over distances of the order of 20–100 Fermi wave lengths λ_F),[28] such that the electron momentum along a direction perpendicular to the surface remains a good quantum number even if the two surfaces are not exactly parallel. If this is not the case, then the quantum formalism (Section II) will naturally pick up those corrugations that take place within the scale of length determined by the Fermi wave length, as illustrated in Figure 17. Consequently, a reasonable estimate for the increase in resistivity induced by electron-surface scattering predicted by the quantum version of FS theory, can be obtained by evaluating the electron self-energy [Equation (14)] for $\delta \approx 0.4\lambda_F, \xi \approx 4\lambda_F$, and using this self-energy to shift the Fermi sphere by adding the corresponding imaginary part to the Fermi wave vector, as described in Section II E. As displayed in Fig. 17, corrugations taking place over scales of length two orders of magnitude larger than λ_F will not scatter electrons significantly, they will only affect the resistivity not because of Quantum Mechanics, but because of the geometrical effect of varying the cross section of the connecting line.

At this point, it seems relevant to point out that a method has been proposed to estimate the cross sectional area of interconnecting lines, by measuring the line resistance as a function of temperature at high (close to or larger than) room temperature.[86–88] The line resistance R data is analysed to determine experimentally dR/dT, and it is assumed that the derivative $d\rho_0/dT$ [where ρ_0 (T) represents the resistivity of the bulk at temperature T associated with the interconnecting line] is given by the known resistivity of the crystalline metal. This brings about the next open question: Is electron-phonon scattering in nanometric metallic interconnects the same as it is in the crystalline metal? Or is there a size effect associated also to this electron scattering mechanism?

B. Is the resistivity arising from electron-phonon scattering also affected by "size effects"?

The resistivity arising from electron-phonon scattering in the Bloch-Grüneisen theory [Equation (1)] depends on the constant A (that is proportional to the electron-phonon coupling constant that characterizes the crystalline lattice), and on the Debye temperature θ that describes the phonon spectrum of the lattice. In the theories of the resistivity induced by size effects presented in Section II, it is assumed that the electron-phonon interaction taking place in nanometric metallic interconnects is the same as that of the crystalline metal and, consequently, the increase in resistivity observed with shrinking dimensions arises only because of electron scattering from defects found in the interconnect that become relevant at smaller scales of length, such as electron scattering by rough surfaces and/or grain boundaries. However, experimental evidence has been recently published suggesting that this assumption may have to be re-examined.

Regarding the electron-phonon coupling constant, it has been measured in gold and silver nanoparticles with sizes ranging 2.2–30 nm embedded in different environments, employing femtosecond pump-probe lasers; a strong increase of the electron-phonon interaction is reported for nanoparticles smaller than 10 nm due to a confinement effect.[89] Therefore, if the interconnect has one or more dimensions that are comparable to or larger than about 10 nm, it would seem unlikely that a significant increase of the coupling constant due to confinement would take place. However, the electron-phonon coupling factor has been measured in Cu films deposited onto Si(100) where the thickness t of the film ranges from 5 nm < t < 1000 nm; an enhancement of the coupling constant was reported for t < 50 nm.[90,91] Hence, this issue may also need to be reexamined.

Regarding the phonon spectrum of a metallic sample of reduced dimensions, it has been suggested that a nanometric sample might exhibit a different phonon spectrum characterized by a smaller Debye temperature θ (a "softer" phonon spectrum), which would provide an increased number of phonons available for electron-phonon scattering at a temperature T, when compared to the number of phonons available in the macroscopic crystalline bulk at the same temperature. There are reports in the literature where the resistivity of metallic films and wires has been measured over a wide temperature range, from 4 K to 300 K, and it has been reported that the slope $d\rho/dT$ of the resistivity of the sample plotted versus temperature T near room temperature is larger than that expected from the bulk crystal;[92–97] in our own work, we have observed repeatedly this increase in the slope $d\rho/dT$ near room temperature.[72] We are not aware of any theoretical study of the phonon spectrum of samples of reduced dimensionality predicting that the Debye temperature for a thin metallic wire or thin film should be smaller than the Debye temperature in the bulk, so this issue also seems to remain open.

C. Modeling of nanoscale devices: Ballistic transport or diffusive transport?

The scientific community interested in size effects in interconnects has experienced a notorious and remarkable change of outlook, regarding the description of charge transport across nanometric metallic interconnects and the modelling of nanoscale devices. After using the classical theory of Mayadas and Shatzkes for decades, without questioning the validity of the physical description underlying the theory, over the last 15 years, a modelling of quantum transport on nanoscopic electronic devices (including transistors and molecular wires) has emerged, based upon Non Equilibrium Green's Functions (NEGF) and the use of the Büttiker-Landauer formalism to calculate the current flowing across the wires.[98–102] Quantum Mechanics is involved in the use of the Büttiker-Landauer formalism and in the calculation of the wave functions describing electrons in the system employing Density Functional Theory (DFT). Within this context, there is a recent report where charge transport on Cu wires (having a diameter of the order of 3 nm or smaller) has been computed using the formalism of Büttiker and Landauer,[6] that is, assuming that electron motion within the wire is well described by a model of *ballistic transport*. This is a quantum model appropriate for describing electron motion in semiconducting structures cooled to 4 K, where the

semiconductor has a very small amount of impurities/defects and the phonons are frozen out. As explained in Ref. 60:

> "…The semiconductor material making up the heterostructure can be made so pure that electrons move ballistically—without undergoing bulk scattering—from one electrode to the opposite electrode. Under such conditions, charge transport is best described in terms of electron waves that propagate through the cavity defined by the macroscopic boundaries that define the electrodes, according to the quantum formalism proposed by Büttiker and Landauer, to describe the conductance of quantum point contacts in terms of the quantum of conductance q^2/h…" (Ref. 60, p. 174).

Although the results obtained by calculating charge transport across nanometric Cu wires provides information that was not available and that is certainly very interesting, the formalism of Buttiker and Landauer does not incorporate either the effect of electron scattering by impurities/point defects or the effect of electron-phonon scattering. Therefore, the distinction between ballistic transport and diffusive transport as the appropriate description of charge transport underlying the formalism employed in the calculation of the current flowing across the interconnect seems relevant; it has been discussed in several text books addressing quantum transport in mesoscopic systems.[102–104]

In the model of ballistic transport, electrons move across the connector unhindered, without undergoing scattering (except when they arrive at the electrodes); *energy dissipation occurs at the electrodes*. On the contrary, in the model of diffusive transport, electron transport occurs noncoherently, for electrons undergo many energy dissipating collisions as they move between the electrodes. The scale of distance that defines when electron transport is ballistic or diffusive, is the distance L_{ph} over which the electron wave function will lose coherence because of electron scattering. If the distance L between the measuring electrodes is such that $L \gg L_{ph}$, then electron transport will be diffusive. On the contrary, if $L < L_{ph}$, electron transport will be ballistic. When $L \approx 3L_{ph}$, important corrections to ballistic transport (arising from electron scattering as they move between the electrodes) are expected. A transition from diffusive to quasiballistic electron transport has been reported in Ag nanowires with decreasing temperature.[105]

The change from diffusive to ballistic transport does not occur only in the case of the wave functions representing electrons, it has also been reported in ultrasound waves propagating in disordered media;[106] a transition from diffusive to ballistic transport is reported when the sample thickness L becomes smaller than about 3ℓ, where ℓ is the transport mean free path (the distance traveled by the ultrasound wave packet between two scattering events).

Ballistic transport is a model appropriate in the (extreme) quantum limit where the sample has been cooled to 4 K so the phonons are frozen out, and where (because of the methods of molecular beam epitaxy used to grow the semiconducting samples), impurities/defects play a negligible role. The model of ballistic transport neglects the energy dissipation taking place when electrons collide with structural defects such as impurities/point defects, grain boundaries, or phonons. In crystalline Cu, $\ell_{Cu}(300) = 38$ nm; so we would expect that the resistivity of a nanometric Cu wire at room temperature computed using the Büttiker-Landauer formalism is roughly correct when $L \approx \ell_{Cu}(300)$, but is underestimated for wires whose length L is larger than about $2.5\ \ell_{Cu}(300) \approx 100$ nm; the underestimation will grow larger with increasing L. Moreover, the experimental information regarding the voltage drop measured on a nanometric scale in Au films[84] and Cu wires[85] at room temperature employing a Scanning Tunneling Potentiometer provides conclusive evidence that energy dissipation takes place across the entire sample and not just at the measuring electrodes; therefore, it contradicts the physical description of charge transport underlying the model based upon the Büttiker-Landauer formalism.

From the engineering point of view, in the last decade, NEGF has been widely used to model transport coefficients for nanodevices (including transistors whose dimensions are way below the electronic mean free path in the semiconductor at room temperature). The transport coefficients in this kind of structures have been modeled considering a ballistic behaviour plus diffusive corrections to account for some (rather infrequent) electron scattering events; the usage of NEGF in these structures seems well justified. However, the question arises regarding which method should be used in a metallic wire connecting these small devices–transistors,

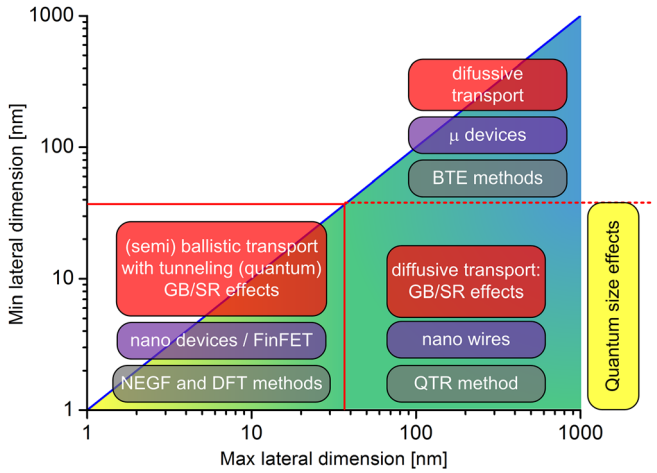

FIG. 25. Schematic representation of the range of validity of different methods employed to calculate charge transport in devices, including interconnects. The ordinate represents the minimum lateral dimension of the device/connector; the abscissa represents the maximum lateral dimension of the device or the length of the interconnect. The solid line in red represents the electronic mean free path in crystalline Cu at 300 K. The upper right corner describes devices in the micrometer range, where charge transport is diffusive, and may be well described by a BTE. In the lower left corner we find devices/connectors where charge transport occurs in the ballistic or quasiballistic regime, and the use of Non Equilibrium Green's Function (NEGF) and of the Density Functional Theory (DFT) is well suited for describing small corrections to the ballistic regime arising from a few electron scattering events taking place between the electrodes. In the lower right hand corner charge transport is diffusive, reflecting the dominance of electron scattering by structural defects such as Grain Boundaries (GB) and rough surfaces (Surface Roughness, SR), well described by the Quantum Theory of Resistivity (QTR) presented here.

whose length can vary from a few nanometers to microns; the increase in the overall resistance of the equivalent circuit has not been addressed so far. The range of validity of different methods used to describe charge transport in nanoscale devices is schematically portrayed in Fig. 25.

The new quantum theory should be used in a specific range of parameters for the Cu nanowires where the length of the wire exceeds about $2\ell_{Cu}(300)$. The resistance seen in the contacts of a transistor may vary from a few ohms to kilo ohms depending on the operation region, while the resistance of a nanowire may increase due to size effects in at least 30% from the bulk resistance; both elements are complementary in the estimation of the RC delay of the overall circuit and cannot be accounted for simply by adding the resistance to the transistor.

D. Shortcomings of the quantum theory of electron-grain boundary scattering

Although the quantum theory of resistivity of metallic interconnects presented in Section II E represents a significant improvement when compared to classical theories based upon the BTE, there are still some important details that the theory does not incorporate. The data available support the notion that the resistivity of Au interconnects (made out of grain whose average diameter is in the range of 10 nm) arises from weak Anderson localization induced by electron scattering from disordered grain boundaries, which gives rise to an Anderson localization length L_{loc} of about 110 nm that controls the resistivity of the specimen. It remains to be proved that the same localization phenomena also takes place in Cu interconnects; we are preparing experiments to answer this question.

However, there are certain elements that are missing from the theory, which will be addressed below.

1. The texture of grain boundaries

In the quantum theory presented in Section II E, the effect of shrinking dimensions of the interconnect is represented within the theory by grains of smaller dimensions. Consequently, the number of grain boundaries found along a mean free path increases as dimensions shrink, and when the average grain diameter becomes smaller than the electronic mean free path at room temperature, electron scattering from disordered grains gives rise to weak Anderson localization, where the localization length is controlled by the degree of disorder.

However, evidence has been published recently indicating that *shrinking dimensions has a rather profound influence in the texture and the distribution of grain boundaries*. There is a recent study of the local texture of Cu interconnects employing diffraction scanning transmission electron microscopy employing a beam with a spatial resolution of less than 5 nm. The results reveal strong variations in texture and grain boundary distribution of Cu lines upon downscaling. Lines of width 1.8 μm exhibit a strong $\langle 111 \rangle$ normal texture and comprise large micron size grains. Upon downscaling to 180 nm, a $\{111\}\ \langle 110 \rangle$ bi-axial texture has been observed. Narrower lines of widths 120 nm and 70 nm reveal sidewall growth of $\{111\}$ grains and a dominant $\langle 110 \rangle$ normal texture. The microstructure in these lines includes clusters of small grains separated by high angle boundaries in the vicinity of large grains.[107]

There are also simulations that suggest that high angle grain boundaries contribute significantly to the resistivity arising from electron-grain boundary scattering.[6,108–110] Representing grains by a sphere that has the same volume as the grain, and grain boundaries by a series of delta function potentials is clearly an over simplification that can certainly be improved upon.

2. The effect of molecules present on a metallic rough surface

Another aspect that has been left out of the quantum theory is how adsorbed molecules might affect electron scattering by the rough surface limiting the interconnect and how coating the metallic film with a different metal might modify the resistivity of the specimen. An interesting manifestation of this is the increase in a few percent of the resistivity observed in thin gold films upon adsorbing self-assembled thiol molecules.[111] This indicates that—beyond the quantum reflectivity [Equations (12) and (14)] determined by the parameters (δ, ξ) describing the Gaussian profile of the surface roughness—the nature of the molecular orbitals characterizing the electron states of the adsorbed molecule has a measurable effect on the reflectivity of the surface and, consequently, on the resistivity of the interconnect. It has also been reported that the resistivity of 9 nm thick Cu films measured *in situ* (in the vacuum evaporation chamber) is *reduced* by 11%–13% when coated with 0.75 nm thick Ni layer.[112]

According to the quantum theory presented above, the quantum reflectivity of the surface seems entirely determined by the geometry of the surface, by the parameters (δ, ξ) that describe the surface roughness. It is not clear how molecules adsorbed on the metallic surface would modify the resistivity of the specimen. It is not clear either, how coating the interconnect with a different metal, might modify its resistivity. Again, there seems to be room for improvement.

ACKNOWLEDGMENTS

We gratefully acknowledge data on Cu wires of rectangular cross section provided by Y. K. Siew, N. Jourdan, I. Ciofi, K. Croes, C. J. Wilson, B. J. Tang, S. Demuyinck, J. Bömmels, and Zs. Tökey from IMEC, Leuven, Belgium, by Z. Wu and H. Ai from Applied Materials, Sunnyvale, California, USA, and by D. Cellier and A. Cockburn from Applied Materials, Leuven, Belgium. We gratefully acknowledge support from Universidad de Chile, Vicerrectoria de Investigacion y Desarrollo, under contract Enlaces Fondecyt ENL 010/16.

[1]A. F. Mayadas and M. Shatzkes, Phys. Rev. B **1**, 1382 (1970).
[2]See http://www.anandtech.com/show/10183/intels-tick-tock-seemingly-dead-becomes-process-architecture-optimization this article discusses the difficulties and complexity of efforts by INTEL to introduce 14 nm node in the fabrication of IC's.
[3]See http://www.anandtech.com/show/9447/intel-10 nm-and-kaby-lake this article portrays the delay by INTEL in introduciong the 14 nm node

into the mass production of IC's, and the prespective of moving into the 10 nm node by 2017 and to the 7 nm node by 2019.
[4]See http://www.technologyreview.es/informatica/49249/los-chips-del-futuro-perderan-velocidad-para/ this article discusses the difficulties arising from Moore's law coming to a halt, that is forcing IC manufacturers such as INTEL to look for fundamentally new technologies such as spintronics for future developments.
[5]See http://www.technologyreview.es/informatica/49783/intel-confirma-el-freno-a-la-lev-de-moore/ this article (published on march 20, 2016) states that INTEL, perhaps the largest manufacturer of ICs, confirms that Moore's law is coming to a halt. *This is remarkable, for it was Gordon Moore (cofounder of INTEL) who proposed this empirical law in 1965*.
[6]S. L. T. Jones, A. Sanchez-Soares, J. J. Plombon, A. P. Kaushik, R. E. Nagle, J. S. Clarke, and J. C. Greer, Phys. Rev. B **92**, 115413 (2015).
[7]C. Arenas, R. Henriquez, L. Moraga, E. Muñoz, and R. C. Munoz, Appl. Surf. Sci. **329**, 184 (2015).
[8]I. Stone, Phys. Rev. **6**, 1 (1898).
[9]D. K. C. MacDonald, Nature **163**, 637 (1949).
[10]R. A. Matula, J. Phys. Chem. Ref. Data **8**, 1147 (1979).
[11]E. H. Sondheimer, Adv. Phys. **1**, 1 (1952).
[12]K. Fuchs, Proc. Cambridge Philos. Soc. **34**, 100 (1938).
[13]M. S. P. Lucas, J. Appl. Phys. **36**, 1632 (1965).
[14]P. A. Badoz, A. Briggs, E. Rosencher, F. A. D'avitaya, and C. D'Anterroches, Appl. Phys. Lett. **51**, 169 (1987).
[15]S. B. Soffer, J. Appl. Phys. **38**, 1710 (1967).
[16]R. B. Dingle, Proc. R. Soc. A **201**, 545 (1950).
[17]K. Sarginson and D. K. C. MacDonald, Nature **164**, 921 (1949).
[18]D. K. C. MacDonald and K. Sarginson, Proc. R. Soc. London A **203**, 223 (1950).
[19]D. K. C. MacDonald, Proc. Roy. Soc. A **63**, 290 (1950).
[20]D. K. C. MacDonald, Philos. Mag. **2**, 97 (1957).
[21]R. G. Chambers, Proc. R. Soc. A **202**, 378 (1950).
[22]R. G. Chambers, Proc. R. Phys. Soc. A **65**, 458 (1952).
[23]R. Courant and D. Hilbert, *Methods of Mathematical Physics* (Inter-science, New York, 1962), Vol. 2, Chap. 2.
[24]Y. H. Kao, Phys. Rev. **138**, A1412 (1965).
[25]Y. S. Way and Y. H. Kao, Phys. Rev. B **5**, 2039 (1972).
[26]D. Calecki, Phys. Rev. B **42**, 6906 (1990).
[27]R. C. Munoz, A. Ramirez, R. Henriquez, J. P. Garcia, G. Kremer, and L. Moraga, Phys. Rev. B **74**, 233402 (2006).
[28]R. C. Munoz, G. Vidal, G. Kremer, L. Moraga, and C. Arenas, J. Phys.: Condens. Matter **11**, L299 (1999).
[29]L. Sheng, D. Y. Xing, and Z. D. Wang, Phys. Rev. B **51**, 7325 (1995).
[30]A. E. Meyerovich and S. Stepaniants, Phys. Rev. B **51**, 17116 (1995).
[31]A. E. Meyerovich and S. Stepaniants, Phys. Rev. Lett. **73**, 316 (1994).
[32]A. E. Meyerovich and S. Stepaniants, J. Phys: Condens. Matter **9**, 4157 (1997).
[33]A. E. Meyerovich and S. Stepaniants, Physica B **284**, 1944 (2000).
[34]A. E. Meyerovich and S. Stepaniants, Phys. Rev. B **58**, 13242 (1998).
[35]A. E. Meyerovich and S. Stepaniants, Phys. Rev. B **60**, 9129 (1999).
[36]A. E. Meyerovich and S. Stepaniants, J. Phys: Condens. Matter **12**, 5575 (2000).
[37]A. E. Meyerovich and I. V. Ponomarev, J. Phys: Condens. Matter **14**, 4287 (2002).
[38]A. E. Meyerovich and I. V. Ponomarev, Phys. Rev. B **65**, 155413 (2002).
[39]A. E. Meyerovich and I. V. Ponomarev, Phys. Rev. B **67**, 165411 (2003).
[40]Y. Y. Cheng and A. E. Meyerovich, Phys. Rev. **B73**, 085404 (2006).
[41]S. Chatterjee and A. E. Meyerovich, Phys. Rev. B **81**, 245409 (2010).
[42]S. Chatterjee and A. E. Meyerovich, Phys. Rev. B **84**, 165432 (2011).
[43]K. M. Leung, Phys. Rev. B **30**, 647 (1984).
[44]C. S. Chu and R. S. Sorbello, Phys. Rev. B **38**, 7260 (1988).
[45]Z. Tesanovic, M. V. Jaric, and S. Maekawa, Phys. Rev. Lett. **57**, 2760 (1986).
[46]Z. J. Tesanovic, Phys. C: Solid State Phys. **20**, L829 (1987).
[47]N. Trivedi and N. W. Aschroft, Phys. Rev. B **38**, 12298 (1988).
[48]R. C. Munoz, G. Kremer, C. Arenas, and L. Moraga, J. Phys.: Condens. Matter **12**, L379 (2000).
[49]R. C. Munoz, G. Vidal, G. Kremer, L. Moraga, C. Arenas, and A. Concha, J. Phys.: Condens. Matter **12**, 2903 (2000).
[50]R. C. Munoz, R. Finger, C. Arenas, G. Kremer, and L. Moraga, Phys. Rev. B **66**, 205401 (2002).
[51]R. C. Munoz, C. A. Gonzalez-Fuentes, R. Henriquez, A. Espinosa, G. Kremer, L. Moraga, A. Ibañez-Landeta, S. Bahamondes, S. Donoso, and M. Flores, J. Appl. Phys. **110**, 023710 (2011).
[52]R. L. Kronig and W. G. Penney, Proc. R. Soc. London Ser. A **130**, 499 (1931).
[53]R. Henriquez, S. Cancino, A. Espinosa, M. Flores, T. Hoffmann, G. Kremer, J. G. Lisoni, L. Moraga, R. Morales, S. Oyarzun, M. A. Suarez, A. Zuñiga, and R. C. Munoz, Phys. Rev. B **82**, 113409 (2010).
[54]C. Kittel, *Introduction to Solid State Physics*, IV ed. (Wiley and Sons, 1971), Chap. 9.
[55]C. Kittel, *Quantum Theory of Solids* (Wiley and Sons, 1963), Chap. 9.
[56]P. W. Anderson, Phys. Rev. **109**, 1492 (1958).
[57]D. J. Thouless, Phys. Rev. Lett. **39**, 1167 (1977).
[58]See D. Thouless, in *Anderson's Localization in the Seventies and Beyond*, edited by E. Abrahams (World Scientific Press, 2010) or any of the other 21 chapters written by researchers working on Anderson localization in 50 Years of Anderson Localization.
[59]S. Chakravarty and A. Schmid, Phys. Rep. **140**, 193 (1986).
[60]R. C. Munoz, J. Mol. Catal. A **228**, 163 (2005).
[61]R. C. Munoz, R. Henriquez, J. P. Garcia, A. M. Moncada, A. Espinosa, M. Robles, G. Kremer, L. Moraga, S. Cancino, J. R. Morales, A. Ramirez, S. Oyarzun, M. A. Suarez, D. Chen, E. Zumelzu, and D. Lizama, J. Phys.: Condens. Matter **18**, 3401 (2006).
[62]R. C. Munoz, M. A. Suarez, S. Oyarzun, R. Henriquez, A. Espinosa, G. Kremer, L. Moraga, S. Cancino, and R. Morales, Phys. Rev. B **81**, 165408 (2010).
[63]S. Oyarzun, R. Henriquez, M. A. Suarez, L. Moraga, G. Kremer, and R. C. Munoz, Appl. Surf. Sci. **289**, 167 (2014).
[64]R. C. Munoz, J. P. Garcia, R. Henriquez, A. M. Moncada, A. Espinosa, M. Robles, G. Kremer, L. Moraga, S. Cancino, J. R. Morales, A. Ramirez, S. Oyarzun, M. A. Suarez, D. Chen, E. Zumelzu, and C. Lizama, Phys. Rev. Lett. **96**, 206803 (2006).
[65]R. Henriquez, L. Moraga, G. Kremer, M. Flores, A. Espinosa, and R. C. Munoz, Appl. Phys. Lett. **102**, 051608 (2013).
[66]R. Henriquez, S. Oyarzun, M. Flores, M. A. Suarez, L. Moraga, G. Kremer, C. A. Gonzalez-Fuentes, M. Robles, and R. C. Munoz, J. Appl. Phys. **108**, 123704 (2010).
[67]A. B. Pippard, *Magnetoresistance in Metals*, Cambridge Studies in Low Temperature Physics (Cambridge University Press, 1989).
[68]J. M. Ziman, *Electrons and Phonons* (Oxford University Press, 2007).
[69]M. E. Robles, C. A. Gonzalez-Fuentes, R. Henriquez, G. Kremer, L. Moraga, S. Oyarzun, M. A. Suarez, M. Flores, and R. C. Munoz, Appl. Surf. Sci. **258**, 3393 (2012).
[70]R. C. Munoz, C. Arenas, G. Kremer, and L. Moraga, J. Phys.: Condens. Matter **15**, L177 (2003).
[71]R. C. Munoz, G. Vidal, M. Mulsow, J. G. Lisoni, C. Arenas, A. Concha, F. Mora, R. Espejo, G. Kremer, L. Moraga, R. Esparza, and P. Haberle, Phys. Rev. B **62**, 4686 (2000).
[72]R. Henriquez, M. Flores, L. Moraga, G. Kremer, C. Gonzalez-Fuentes, and R. C. Munoz, Appl. Surf. Sci. **273**, 315 (2013).
[73]Y. K. Siew, N. Jourdan, I. Ciofi, K. Croes, C. J. Wilson, B. J. Tang, S. Demuynck, Z. Wu, H. Ai, D. Cellier, A. Cockburn, J. Bömmels, and Zs. Tökey, "Cu wire resistance improvement using Mn-based self-formed barriers," private communication (2015).
[74]R. L. Graham, G. B. Alers, T. Mountsier, N. Shamma, S. Dhuey, S. Cabrini, R. H. Geiss, D. T. Read, and S. Peddeti, Appl. Phys. Lett. **96**, 042116 (2010).
[75]W. Zhang, S. H. Brongersma, Z. Li, D. Li, O. Richard, and K. Maex, J. Appl. Phys. **101**, 063703 (2007).
[76]P. I. Wang, M. D. Frey, M. Washington, S. Nayak, and T. M. Lu, Thin Solid Films **520**, 6106 (2012).
[77]T. Sun, B. Yao, A. P. Warren, V. Kumar, S. Roberts, K. Barmak, and K. R. Coffey, J. Vac. Sci. Technol. A **26**, 605 (2008).
[78]T. Sun, B. Yao, A. P. Warren, K. Barmak, M. F. Toney, R. E. Peale, and K. R. Coffey, Phys. Rev. B **79**, 041402(R) (2009).
[79]T. Sun, B. Yao, A. P. Warren, K. Barmak, M. F. Toney, R. E. Peale, and K. R. Coffey, Phys. Rev. B **81**, 155454 (2010).
[80]K. Barmak, A. Darbal, K. J. Ganesh, P. J. Ferreira, J. M. Rickman, T. Sun, B. Yao, A. P. Warren, and K. R. Coffey, J. Vac. Sci. Technol. A **32**, 061503 (2014).
[81]W. Zhang, S. H. Brongersma, T. Clarysse, V. Terzieva, E. Resseel, W. Vandervorst, and K. Maex, J. Vac. Sci. Technol. B **22**, 1830 (2004).
[82]E. V. Barnat, D. Nagakura, P. I. Wang, and T. M. Lu, J. Appl. Phys. **91**, 1667 (2002).
[83]W. Wu, S. H. Brongersma, T. Clarysse, M. Van Hove, and K. Maex, Appl. Phys. Lett. **84**, 2838 (2004).

[84]M. A. Schneider, M. Wenderoth, A. J. Heinrich, M. A. Rosentreter, and R. G. Ulbrich, Appl. Phys. Lett. **69**, 1327 (1996).
[85]T. H. Kim, X. G. Zhang, D. M. Nicholson, B. M. Evans, N. S. Kulkarni, B. Radhakrishnan, E. A. Kenik, and A. P. Li, Nano Lett. **10**, 3096 (2010).
[86]D. Josell, S. H. Bronsgerma, and Z. Tokei, Ann. Rev. Mater. Res. **39**, 489 (2009).
[87]H. Li, S. Jin, J. Proost, M. Van Hove, L. Froyen, and K. Maex, in *Proceedings of the XIII Conference ULSI Technology* (1998), p. 197.
[88]A. E. Yarimbiyik, H. A. Schafft, R. A. Allen, M. D. Vaudin, and M. E. Zaghloul, Microelectron. Reliab. **49**, 127 (2009).
[89]A. Arbouet, C. Voisin, D. Christofilos, P. Langot, N. Del Fatti, F. Valleé, J. Lermé, G. Celep, E. Cotancin, M. Gaudri, M. Pellarin, M. Broyer, M. Maillard, M. Pileni, and M. Treguer, Phys. Rev. Let. **90**, 177401 (2003).
[90]Y. K. Timalsina, X. Shen, G. Boruchowitz, Z. Fu, G. Qian, M. Yamaguchi, G. C. Wang, K. M. Lewis, and T. M. Lu, Appl. Phys. Let. **103**, 191602 (2013).
[91]X. Shen, Y. P. Timalsina, T. M. Lu, and M. Yamaguchi, Phys. Rev. B **91**, 045129 (2015).
[92]P. M. Th. M. Van Attekum, P. H. Woerlee, G. C. Verkade, and A. A. M. Hoeben, Phys. Rev. B **29**, 645 (1984).
[93]G. Kastle, H. G. Boyen, A. Schröder, A. Plettl, and P. Ziemann, Phys. Rev. B **70**, 165414 (2004).
[94]A. Bid, A. Bora, and A. K. Raychaudhuri, Phys. Rev. B **74**, 035426 (2006).
[95]A. Bid, A. Bora, and A. K. Raychaudhuri, J. Nanosci. Nanotechnol. **7**, 1867 (2007).
[96]Z. Cheng, L. J. Liu, S. Xu, M. Lu, and X. W. Wang, Sci. Rep. **5**, 10718 (2015).
[97]M. M. Kolesnik-Gray, S. Hansel, M. Boese, and V. Krstic, Solid State Commun. **202**, 48 (2015).
[98]J. Taylor, H. Guo, and J. Wang, Phys. Rev. B **63**, 245407 (2001).
[99]M. Paulsson and M. Brandbyge, Phys. Rev. B **76**, 115117 (2007).
[100]M. P. Anantram, M. S. Lundstrom, and D. E. Nikonov, Proc. IEEE **96**, 1511 (2008).
[101]K. H. Bevan, H. Guo, E. D. Williams, and Z. Zhang, Phys. Rev. B **81**, 235416 (2010).
[102]S. Datta, *Electronic Transport in Mesoscopic Systems*, 9th ed. (Cambridge University Press, 2012). Landauer-Buttiker formalism, coherent and non coherent transport discussed in Chap. 2. Non Equilibrium Green's Function discussed in Chap. 8.
[103]S. Datta, *Lessons from Nanoelectronics: A New Perspective on Transport*, Ballistic and Diffusive Transport Discussed in Lecture 4 (World Scientific, 2012).
[104]S. Datta, *Quantum Transport: Atom to Transistor*, 1st ed. (Cambridge University Press, 2013). Coherent transport discussed in Chap. 9, Non coherent transport discussed in Chap. 10.
[105]D. Kojda, R. Mitdank, M. Handwerg, A. Mogilatenko, M. Albrecht, Z. Wang, J. Ruhhammer, M. Kroener, P. Woias, and S. F. Fisher, Phys. Rev. B **91**, 024302 (2015).
[106]Z. Q. Zhang, I. P. Jones, H. P. Schriemer, J. H. Page, D. A. Weitz, and P. Sheng, Phys. Rev. E **60**, 4843 (1999).
[107]K. J. Ganesh, A. D. Darbal, S. Rajasekhara, G. S. Roher, K. Barmak, and P. J. Ferreira, Nanotechnology **23**, 135702 (2012).
[108]B. Feldman, S. Park, M. Haverty, S. Shankar, and S. T. Dunham, Phys. Status Solidi B **247**, 1791 (2010).
[109]B. H. Zhou, Y. Xu, S. Wang, G. H. Zhou, and K. Xia, Solid State Commun. **150**, 1422 (2010).
[110]J. M. Rickman and K. Barmack, J. Appl. Phys. **114**, 133703 (2013).
[111]J. Correa-Puerta, V. Del Campo, R. Henriquez, and P. Haberle, Thin Solid Films **570**, 150 (2014).
[112]P. Y. Zheng, R. P. Deng, and D. Gall, Appl. Phys. Lett. **105**, 131603 (2014).
[113]G. Palasantzas, Phys. Rev. B **58**, 9685 (1998).